Investigation of Transport Mechanisms for n–p–n InP/InGaAs/InP Double Heterojunction Bipolar Transistors

by

Jianqing He

Thesis submitted to the faculty of the

Virginia Polytechnic Institute and State University

in partial fulfillment of the requirements for the degree of

Master of Science

in

Electrical Engineering

APPROVED:

Dr. Aicha Elshabini–Riad, chairperson

Dr. Sedki M. Riad

Dr. E. A. Manus

January, 1989

Blacksburg, Virginia

Investigation of Transport Mechanisms

for InP/InGaAs/InP n-p-n Double

Heterojunction Bipolar Transistors

by

Jianqing He

A. Elshabini-Riad, chairperson

Electrical Engineering

(ABSTRACT)

A more complete model for InP/InGaAs Double Heterojunction Bipolar Transistors (DHBT) is obtained in this thesis by physically analyzing the transport process of the main current components. The potential distribution of the energy barrier constitutes a fundamental analytical concept and is employed for applying the diffusion, the thermionic emission, and the tunneling theories in investigating the injection mechanisms at the e-b heterojunction interface. The diffusion transport is considered first for electron injection from the emitter into the base. The thermionic emission is applied properly at the point of maximum potential energy as one of the boundary conditions at that interface. A suitable energy level is selected with respect to which the energy barrier expression is expanded for the calculation of the tunneling probability. The first "spike" at the conduction band discontinuity is described as the potential energy for the injected electrons to obtain kinetic energy to move into the base region with a substantially high velocity. The electron blocking action of the second "spike" at the b-c junction is also analyzed by considering the transport velocity with which electrons are swept out of that boundary. Based on the material parameters recently reported for both InP and InGaAs, computations of the current components are carried out to provide ß characteristics in good agreement with the reported experimental results.

Acknowledgements

I would like to take this opportunity to thank everyone who has helped me to finish this thesis. I would especially like to express my sincere gratitude and appreciation to Professor A. Elshabini-Riad, my advisor and chairperson of the graduate committee, for her knowledgeable guidance and valuable time spent on beneficial discussion. Without her help, this thesis could not have been completed.

I would like to extend my thanks to Dr. Sedki M. Riad and Dr. E. A. Manus for their helpful suggestions and for serving on the graduate committee.

I deeply wish to thank my dear wife, for her understanding and assistance in many ways, which are necessary to the successful completion of this thesis.

I finally thank my parents for their unfailing love and continuous support, which are essential for me to complete this thesis.

Contents

List of Illustrations and Table

CHAPTER I

Introduction

1.0 Introduction

As a definition, a semiconductor heterojunction is a junction formed by two different dissimilar semiconductors. If the two semiconductors with the same type of conductivity (n–n or p–p) are used to form such a junction, it is called an isotype heterojunction. If the two semiconductors with different type of conductivity (p–n or n–p) are used, the junction is called anisotype heterojunction. The introduction of heterojunctions makes it possible to realize electronic devices including high quality lasers [1,2], optical detectors [3], and modulated-doped FETs [4]. The recent breakthrough in heterojunction applications is the successful realization of high speed and high gain heterojunction bipolar transistors(HBT).

1.1 An Overview of Heterojunction Bipolar Transistors(HBT)

The introductory concept of heterojunction bipolar transistor is basically a wide–gap emitter transistor, originally proposed by Shockley in 1951 [5]. Later, Kroemer analyzed a heterojunction as a wide–gap emitter of a transistor [6]. Unfortunately, this device concept did not come into reality until early 70's because of limitations of technology. The emergence of liquid-phase epitaxy (LPE) as a technology for III-V compound semiconductors resulted in the possibility to bring heterojunction bipolar transistors into reality. Development of molecular beam epitaxy (MBE) and metal–organic chemical vapor deposition (MOCVD) enabled the precise control of composition and impurity doping over small distances of the

order of 50 to 100 Å. The above two technologies led to great progress in HBTs.

Currently, lattice–matched material systems mostly used for HBTs are usually Aluminum Gallium Arsenide(AlGaAs)/Gallium Arsenide(GaAs) and Indium Phosphide(InP)/Indium Gallium Arsenide (InGaAs). The criterion for a good material pairs for HBTs application is a close lattice matching. The reason can be attributed to the great concern of the existence of interface states, which result in numerous recombination centers causing a severe degradation in the current gain. For an AlGaAs/GaAs heterojunction, densities of interface states less than 10^{11} cm $^{-2}$ can be achieved [7]. However, the density of interface states for an InP/InGaAs is much smaller than that for an AlGaAs/GaAs [8].

In conventional homojunction transistors, a tradeoff between the emitter efficiency and the frequency response exists for consideration of the emitter–base junction. In order to achieve a significant injection efficiency γ for an n–p–n transistor, the hole injection current component I_{pe} from the base into the emitter needs to be reduced. This can be achieved by increasing the ratio of the emitter doping to the base doping. Nevertheess, the emitter doping is limited by the solid solubility and heavily–doped effects. In addition, the reduction of the base doping causes a large base resistance, which degrades the high frequency performance of the transistor. In contrast to the homojunction case, the valence band discontinuity ΔE_c for a heterojunction transistor acts as a hole barrier that suppresses the hole injection. As a result, a high current gain can be obtained without any sacrifice of low base resistance. Therefore, excellent high frequency performance of HBTs results in conjunction with good emitter injection efficiency.

Advanced technologies, such as MBE and MOCVE, possess the capability of achieving a base width less than 0.1 μm. The great reduction of the base width leads to a great reduction of the transit time within the base region. Since the base transit time is a dominant factor limiting the high frequency performance of the transistor, a heterojunction bipolar transistor(HBT) with a thin base can have a high cut–off frequency exceeding 100 GHz [9]. Numerical simulations suggest a near–ballistic transport when the base region is less than 1000 Å and a quasi–electric field of about 20 kv/cm exists [10,11]. A ballistic transport means collision–free transit over distances shorter than a mean free path for the particular electron energy. In HBTs, an important factor to achieve near–ballistic transport is the presence of the "spike", the conduction band discontinuity ΔE_C. This extra potential energy barrier can launch the injected electrons into the base region with a substantial kinetic energy and hence with a very high velocity [12].

The "spike" occurs due to the abrupt junction nature. Although the "spike" has some advantages as mentioned above, there are some drawbacks caused by the "notch", which accompanies the occurrence of the "spike". The "notch" collects injected electrons and hence enhances the recombination losses. It is desirable to eliminate the notch by growing a graded junction, which yields smoothly and monotonically varying band edges, thus avoiding the effect. Some researchers explain that the graded junction possesses an additional advantage over the abrupt junction, a higher ratio of electron to hole current or higher injection efficiency[13]. The controversy about the benefit of the graded junction versus the abrupt junction, or vice versa, focuses on the achievement of a large valence band discontinuity ΔE_V. For an AlGaAs material system, the valence band discontinuity, ΔE_V, is quite small($\Delta E_V = 0.15\ \Delta E_g$). Therefore, the graded junction is usually used in such a

material system. However, when the device speed is the main concern, an abrupt junction is often desirable [14]. Actually, the principal benefit of heterojunction transistors is not the ability to achieve high current gain, but the flexibility of doping levels variations in both the emitter and base regions without any significant sacrifice of injection efficiency, and then to design a well–optimized transistor with consideration at a higher performance level [12].

Future potential of HBTs lies in the possibility of incorporating the devices into ICs in the near future. Currently, the main interest in HBTs tends to be in highly integrated digital switching transistors. Such application suggests Double Heterojunction Bipolar Transistors (DHBT), meaning a wide–gap collector [12,15]. There are several excellent advantages for DHBTs. First, hole injection from the base into the collector in digital switching applications under conditions of saturation can be suppressed. Second, emitter/collector can be interchangeable, by simply changing the bias conditions, making great improvement on ICs design architecture and high speed switching performance. Moreover, optimization of base and collector can be separated. This is especially important in microwave power transistors, in which hole mobility is required to be high to achieve low base resistance. For a microwave power transistor, the transit time through the collector region is dominant, as compared to the one through the base. Design of DHBTs can make it possible to employ a material with high electron mobility, such as InP, as collector to obtain a small transit time through collector. A DHBT made of InP/InGaAs/InP was reported. Such a transistor exhibits an near-ideal β versus I_C characteristic, which means current gain independent of the on collector current. Therefore, DHBTs possess a very promising future in high performance transistors and in ICs applications.

The largest benefit, as mentioned above, of HBTs is the ability to have freedom to select the doping concentration in the emitter and the base regions while a reasonably–high current gain can still be achieved. This benefit gives rise to optimization of the emitter capacitance and the base resistance, which are critical factors affecting the upper cutoff frequency and the high speed performance of microwave transistors. It is well known that a junction capacitance of a unsymmetrically doped p–n junction depends on the doping level of the lightly doped side. Since the emitter side can be doped less than that of the base side, the emitter capacitance now can rely on the emitter doping level and can be decreased. Also, reduction of the emitter capacitance can improve the noise figure significantly in small–signal microwave amplification. The most important change made by HBTs is the great reduction of base resistance due to the highly–doped base. This is because both the maximum oscillation frequency f_{max} for microwave transistors and the switching time constant for switching transistors are strong function of the base resistance R_b. Obviously, HBTs are considered excellent candidates for microwave and high speed switching applications.

Since the advent of HBTs, a lot of efforts have been done on modeling, where focus is on the heterointerface and its effects on the transistor behaviors. Difficulties of modeling arise from the interface due to the transition between the two materials [16]. This transition causes energy discontinuities in both the conduction band and the valence band, producing complicated energy band structure. Also, the effects of the extra energy potential barriers on the transistor behaviors are of great concern. The work of modeling HBTs roughly falls into two classes. One class is directed to model the carrier transport processes within the transistor and to relate the device's physical parameters and structural parameters to the terminal parame-

ters. Another class is pointed at the electrical model represented by lumped elements using characterization techniques, in which the transistor is considered as a "black box". It is undoubted that computers and the related software packages play important roles in modeling HBTs. So far, no complete model exists that can describe satisfactorily in describing HBTs. Therefore, investigation of the carrier transport processes within a typical heterojunction bipolar transistor and construction of an electrical network model through microwave characterization are primary concerns in this thesis.

1.2 Research Objectives

The main interest in modeling HBTs lies in correctly and accurately describing the carriers transport mechanisms across the energy barriers caused by the discontinuities. The models for homojunction transistors cannot be directly applied to HBTs.

Several models for HBTs have been proposed using similar methods to those used in the metal–semiconductor barrier case due to the fact that metal–semiconductor structure constitutes a type of heterostructure [17,18]. These models include the thermionic model, the thermionic–diffusion model, and the thermionic–field– diffusion model for AlGaAs/GaAs HBTs. Researchers have also proposed the current balancing concept, where the current transport mechanism across an interface is treated as two–step process, a thermionic emission process followed by Schockley diffusion process.

Examining the literature research, the following questions need to be addressed and problems investigated:

1. Whether the convectional boundary conditions for homojunction transistors are applicable to HBTs? The referred conditions are usually the equations for the injected carrier concentrations $n_{pb} = n_{po} \exp(qV_{be}/kT)$ and $p_{nb} = p_{no} \exp(qV_{be}/kT)$, where n_{po} and p_{no} refer to the equilibrium electron and hole concentrations, respectively, in the p–region and n–region.

2. How should the energy barrier be correctly treated for the conduction discontinuity?

3. How should the conduction band–to–band or direct tunneling be taken into consideration?

4. What are the effects of a short base width and the second "spike" for a DHBT on the carriers transport process?

5. What can be obtained for a InP/InGaAs/InP DHBT if the above considerations are taken?

6. Is it possible to propose an electrical network model by using lumped elements for future characterization?

Addressing these questions and attempting to answer them consists of the research objectives of this thesis. The study in this thesis is basically theoretical. The main reason for this is due to the lack of facilities for making samples and nonavailability of commercial devices. Therefore, experiments are left to be done in future.

The thesis consists of five chapters. Chapter I is a general introduction that overviews the development of HBTs and outlines the main research objectives. Chapter II provides the basic theory of heterojunctions. Chapter III introduces the fundamental concepts of Heterojunction Bipolar Transistors. Chapter IV is the main core of the thesis, in which the transport mechanisms are investigated and

simulated. Chapter V summarizes the main concerns of HBTs in microwave applications, Providing a theoretical basis for future work as suggested in the following chapter. Chapter VI is a general conclusion summarizing the main findings of the thesis, and directions for future work.

CHAPTER II

The Basic Theory of Heterojunction

2.0 Introduction

In general, any contact between two different materials in the sense of electrical properties consist of a heterojunction. The heterojunctions of most interest are those between two different semiconductor materials as well as those between a metal and a semiconductor. The concern in this thesis is to thoroughly study the heterojunction between two different III–V compound semiconductor materials.

2.1 Formation of Heterojunction

Conceptually, when two semiconductors with different band gaps and other material parameters are brought into contact, a heterojunction is formed. However, it took almost thirty years to practically and successfully realize this concept. The successful realization of heterojunctions is attributed to the advances of epitaxial technologies, especially MBE and MOCVD. These two technologies are capable of accurately growing and controlling the epitaxial layers and the doping process. A schematic diagram of the MBE technique is shown in Figure 2.1. Using MBE, a layer of III–V semiconductor is epitaxially grown on top of different semiconductor material. A list of various band gaps of III–V semiconductors is given in Figure 2.2 [19]. One can observe that band gaps vary with the variation of compositions of materials. Therefore, a graded heterojunction is formed if the composition of one of the two materials is varied during the growing process. Otherwise, an abrupt

heterojunction is achieved. The doping is accomplished at the same time as the epitaxial layers growth.

In order to form a high quality heterojunction, the two materials must have a similar crystal structure and a closely–matched lattice spacing. Two materials with different crystal structures result in crystal dislocations. Mismatched lattice between two materials result in "dangling bonds". These defects become harmful recombination traps, producing undesirable recombination current. Therefore, the selection of lattice–matched material pairs is a very critical factor for successful heterojunction formation.

2.2 Energy Band Diagram of Typical Heterojunctions[20,21]

For a typical n–p heterojunction, it is assumed that the two materials have different band gaps E_g, different permittivities ϵ, different work functions ϕ_m, and different electron affinities χ. When the materials are separated initially, their energy band diagram can be illustrated in Figure 2.3. As the case in a homojunction, when the separated semiconductors are brought together, their Fermi levels have to line up and the energy band of the transition region is smooth. For a heterojunction, when the requirement of lining–up Fermi levels is satisfied, there have to exist discontinuities in both the conduction band and the valence band. These discontinuities are represented by ΔE_c and ΔE_v, respectively. The resulting energy band diagram is shown in Figure 2.4. It is noted that this is the case of an abrupt junction. Since the vacuum level is continuous everywhere and parallel to the band edge, ΔE_C is equal to $(\chi_1 - \chi_2) = \Delta\chi$. The related parameters are also shown in the Figure.

Besides the shown n–p heterojunction, there are three other heterojunctions

with different configurations. They are p–n heterojunction, n–n heterojunction, and p–p heterojunction. Their energy band diagrams are shown in Figure 2.5.

2.3 Physical Parameters For A Heterojunction

To describe a heterojunction, the following physical parameters are often used:

ϕ_S: work function which is defined as the energy required to remove an electron from the Fermi level to the vacuum level.

χ: electron affinity which is defined as the energy required to remove an electron the bottom to the vacuum level.

ΔE_c: discontinuity of the conduction band. As an empirical quantity, ΔE_c is equal to $\Delta E_c = (\chi_2 - \chi_1) = \Delta\chi$.

ΔE_v: discontinuity of the valence band, which can be given as $\Delta E_v = (E_{g1} - E_{g2}) - \Delta\chi$.

V_{bi}: The total built–in potential voltage, which is the sum of the partial built–in voltage ($V_{bi1} + V_{bi2}$), where V_{bi2} and V_{bi2} are the electrostatic potentials at equilibrium in semiconductor 1 and semiconductor 2, respectively.

$\psi_{(x)}$: potential distribution, which is often obtained by solving Poisson's equation.

$\varepsilon(x)$: electric field distribution, which is also obtained from solving Poisson's equation.

$\Delta a_0/a_0$: relative lattice mismatch rate, where a_0 is the crystal lattice constant of semiconductor material.

2.4 Several Important Formula For p–n Heterojunction[20,21]

The major difference, caused by different material parameters, between a homojunction and a heterojunction lies in the interface. For each side of a heterojunction, the equations and methods applied to a homojunction are still applicable to the heterojunction. Although there are energy discontinuities in the transition region, the continuity of electric displacement at the interface holds:

$$D_1 = D_2 \quad \text{or} \quad \epsilon_1 E_1 = \epsilon_2 E_2 \tag{2–1}$$

The above equation can be used as one boundary condition for the solution of Poisson's equation in order to obtain the depletion widths on each side of the heterojunction:

$$x_1 = \left[\frac{2N_{A2}\epsilon_1\epsilon_2(V_{bi} - V)}{qN_{D1}(\epsilon_1 N_{D1} + \epsilon_2 N_{A2})}\right]^{\frac{1}{2}} \tag{2–2}$$

and,

$$x_2 = \left[\frac{2N_{D1}\epsilon_1\epsilon_2(V_{bi} - V)}{qN_{A2}(\epsilon_1 N_{D1} + \epsilon_2 N_{A2})}\right]^{\frac{1}{2}} \tag{2–3}$$

where V is the applied voltage, N_{d1} and N_{A2} are the doping concentrations on the

n–side and p–side, respectively. The depletion capacitance is given by:

$$C = \left[\frac{N_{D1}N_{A2}\epsilon_1\epsilon_2}{2(\epsilon_1 N_{D1} + \epsilon_2 N_{A2})(V_{bi} - V)}\right]^{\frac{1}{2}} \qquad (2-4)$$

The relative voltage supported in each semiconductor is:

$$\frac{V_{bi1} - V_1}{V_{bi2} - V_2} = \frac{N_{A2}\epsilon_2}{N_{D1}\epsilon_1} \qquad (2-5)$$

where $V_1 + V_2 = V$, and V_{bi1} and V_{bi2} are given by:

$$V_{bi1} = N_{D1}x_1/2\epsilon_1 \qquad (2-6)$$

$$V_{bi2} = N_{A2}x_2/2\epsilon_2 \qquad (2-7)$$

It is obvious that the above expressions can be reduced to those for a homojunction when both material sides are set to be the same.

2.5 Two Important Material Pairs for Heterojunctions

Usually, there are several rules as a guide to select material pairs for heterojunctions. These rules include a) Select the prime semiconductor of the active region with the required consideration of the band-gap and the mobility; b) Select the paired semiconductors which possess a very close lattice constant; c) Select the paired materials which can be fabricated without having technological compatibility and severe cross–doping problems. Nowadays, there are two important material pairs for HBTs applications, AlGaAs/GaAs and InGaAs/InP.

From the diagram Figure 2.2, the energy gap versus lattice constant for wide

range of ternary and binary III–V and II–VI compound semiconductors, one can observe that GaAs has a lattice constant of 5.653 Å with a band-gap of 1.424 ev at room temperature. Also it is known that AlAs has a very close lattice constant but with a quite different band–gap of about 2.1 ev. The band–gap of AlGaAs can be changed, without changing the lattice constant, to obtain a desirable value for HBTs by changing Ga fraction. The electron mobility of GaAs, which serves as the active base in HBTs, can reach up to 8500 $cm^2/v–s$. In general, AlGaAs is grown on GaAs in order to achieve a good interface. The discontinuity of the valence band ΔE_v is about $0.44\Delta E_g$ and the discontinuity of the conduction band ΔE_c is about $0.62\Delta E_g$. ΔE_v and ΔE_c are of great concern in the HBTs design. This point will be discussed in details in the following chapter III. The interface traps, spread over a distance of about 140 Å on the GaAs side, is about 2×10^{16} cm^{-3} and the capture cross section σ is 8×10^{15} cm^2, implying an interfacial recombination velocity of 10^4 cm/s[19].

InP has a lattice constant of 5.8686 Å with a energy band–gap of 1.35 ev. $In_xGa_{1-x}As$ is found to have a close lattice constant to InP but with a different band–gap of about 0.75 ev when the fraction factor $x = 0.53$. In other words, $In_{.53}Ga_{.47}As$ is closely lattice–matched to InP. There are several reasons for selection of this material system. The main reason is that it has an extremely low base transit time due to the high electron mobility[22], about 1.1×10^4 $cm^2/v–s$, in InGaAs which is used as the active base. Second, the energy band–gap of InGaAs is compatible with second generation optical communication system, in which 1.1 - 1.6μm wavelength range is used. Third, InGaAs possesses favorable energy band discontinuity: $\Delta E_c = 0.39\Delta E_g$ and $\Delta E_v = 0.61\Delta E_g$ [23,24]. Furthermore, This material system has lower surface recombination(a factor of 100 smaller than AlGaAs/GaAs system) [8], producing excellent β — I_c characteristic. Other

properties such as low ohmic contact resistance and excellent interface quality make InGaAs/InP HBTs a strong competitor to AlGaAs/GaAs HBTs. The main difficulties for InGaAs/InP system lie in growing technology: it is difficult to grow P bearing compounds by MBE and control of p–type dopants by MOCVD [23].

2.6 Conclusion

A heterojunction is formed by two semiconductors which differ in material and/or conductivity type. The main difference between a heterojunction and a homojunction in their energy bands is the existence of the conduction band discontinuity and the valence band discontinuity in the heterojunction. The primary concern of selection of the materials for heterojunction pair is the lattice matching. A good heterojunction pair is the one which possesses a very close lattice constant. The mostly common heterojunction pairs are AlGaAs/GaAs and InGaAs/InP.

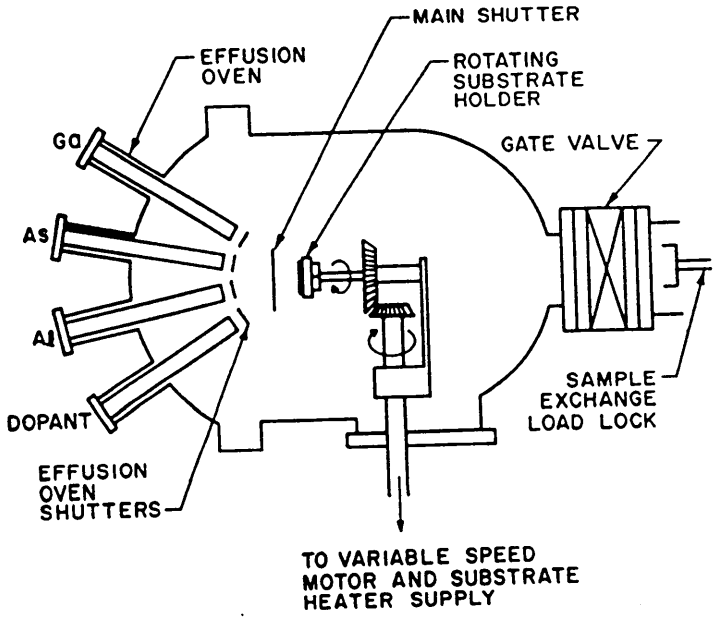

Figure 2.1 Schematic of a Molecular–Beam Epitaxial system.

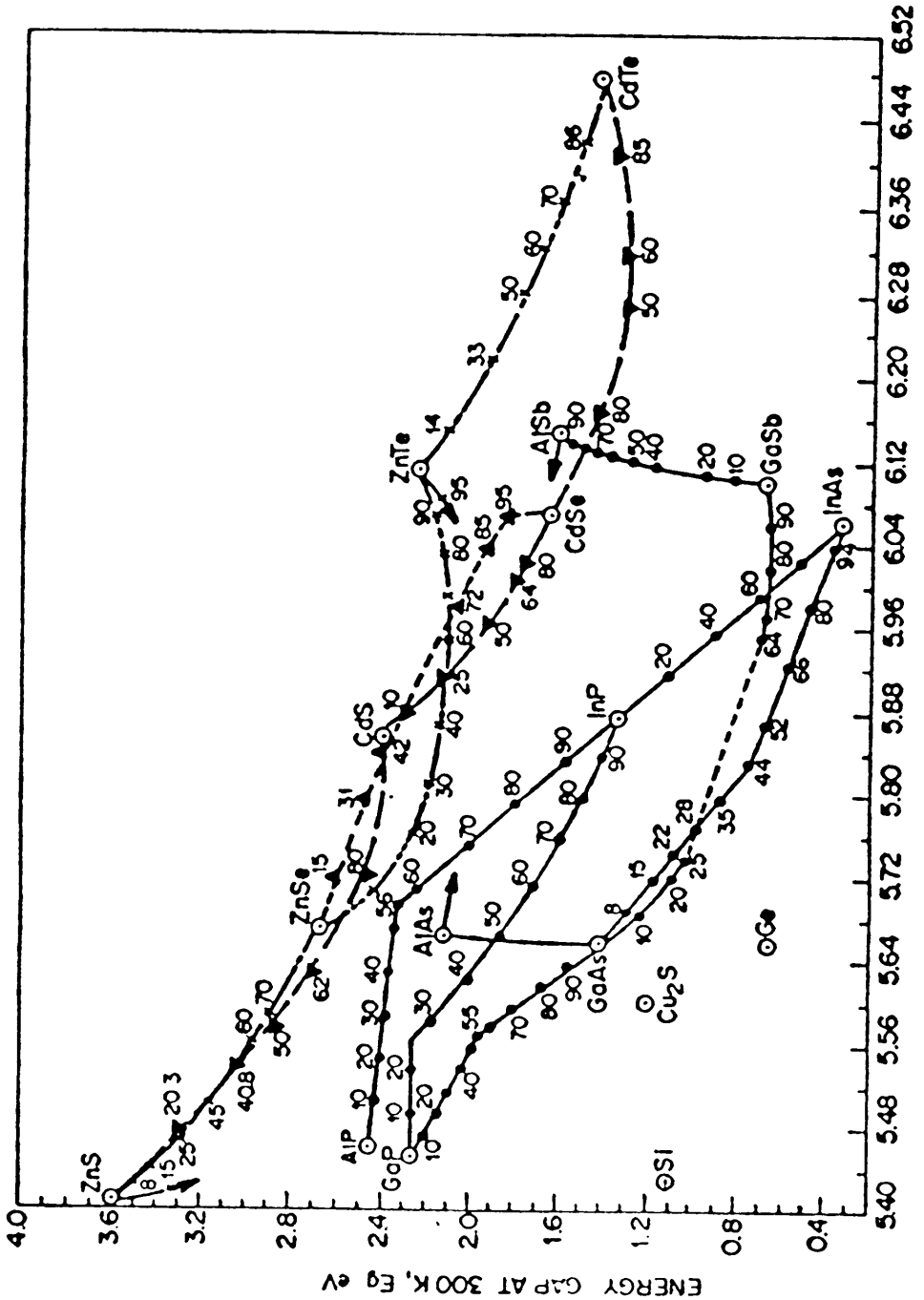

Figure 2.2 Energy gap versus lattice constant for III–V and II–V semiconductors

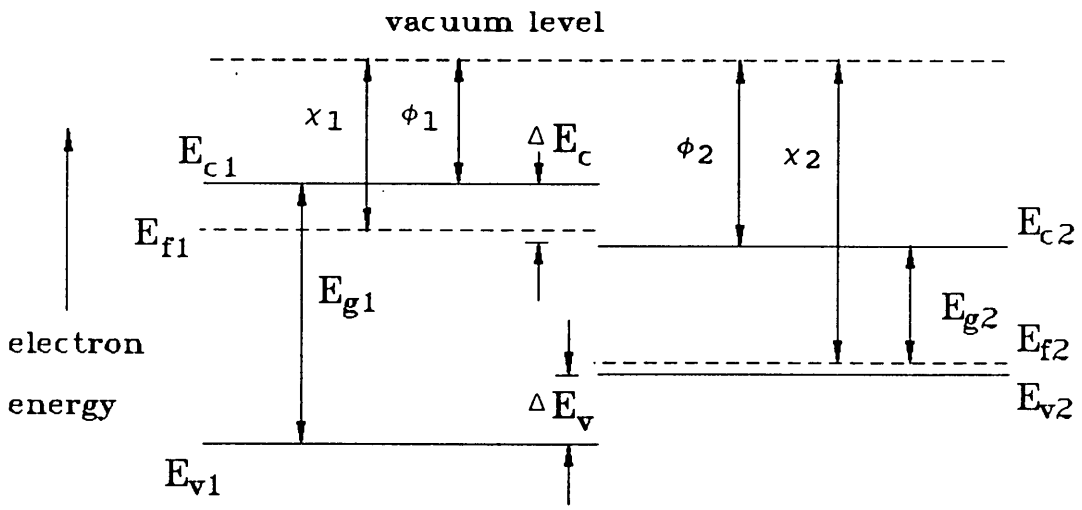

Figure 2.3 Energy Diagram for two Isolated Semiconductors

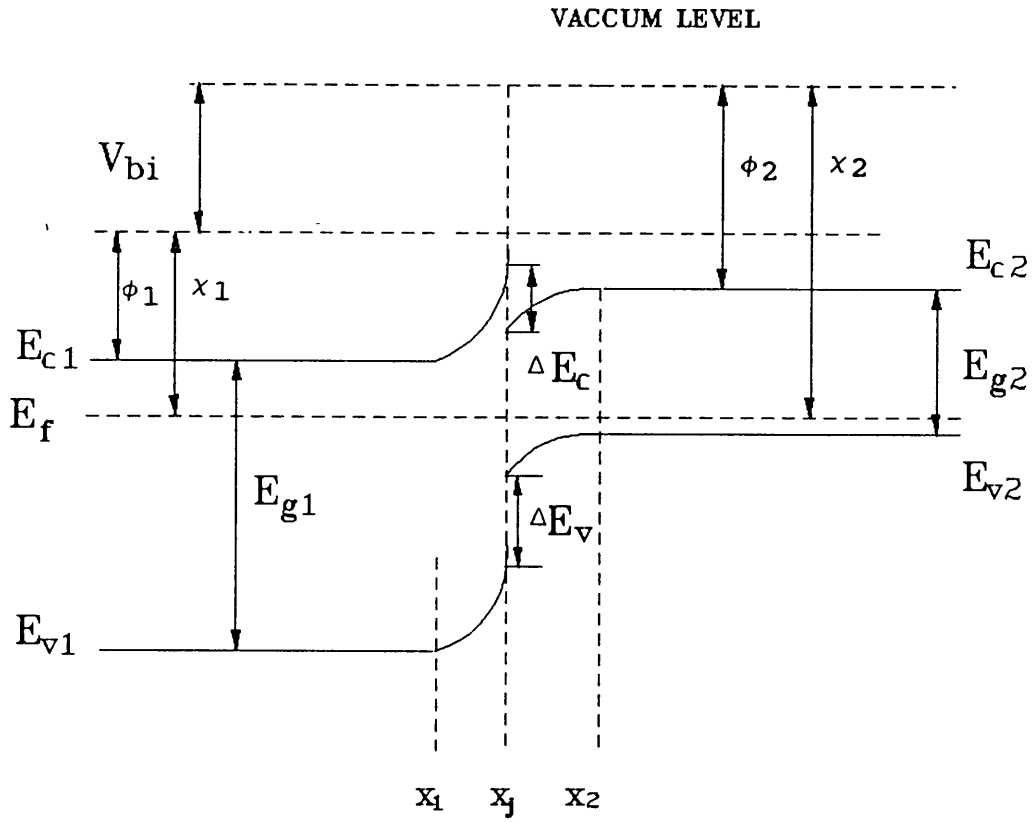

Figure 2.4 Energy Band Diagram of an Ideal n p anisotype heterojunction at thermal equilibrium

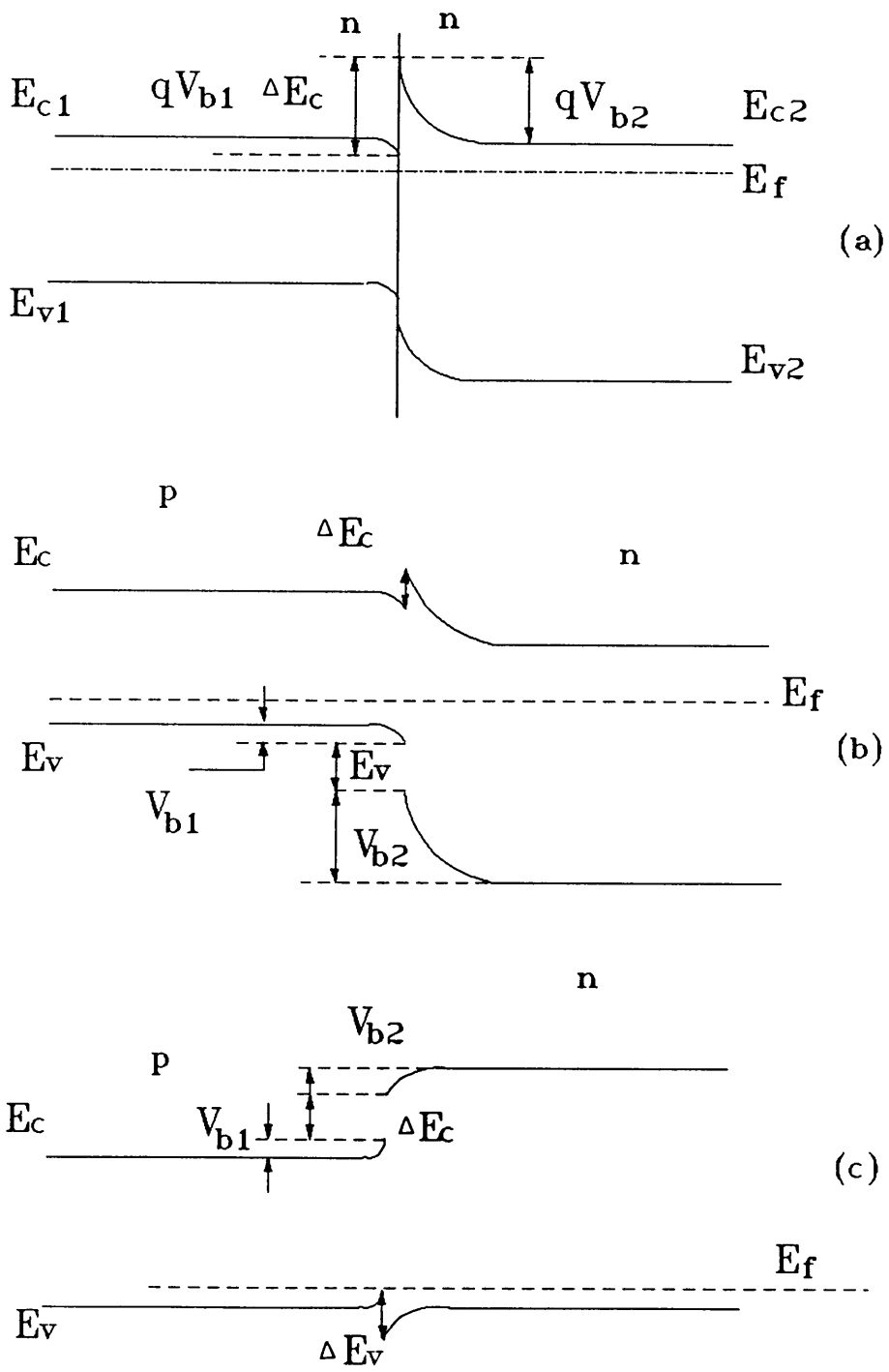

Figure 2.5

Energy Band Diagrams for Ideal n-n, p-n, p-p Heterojunctions, respectively.

CHAPTER III

Fundamental Concepts of Heterojunction Bipolar Transistors

3.0 Introduction

In this chapter, the fundamental concepts are to be introduced. As the original concept, wide-gap emitter transistor is first described. The basic principle of heterojunction is given to provide the insight of effects caused by the variation of energy gap on the carrier transport. The effects of the discontinuities in both the conduction band and the valence band are briefly analyzed. The concept of Double Heterojunction Bipolar Transistor and the experimental results reported by other researchers are presented to form the basis of the following chapter.

As an introductory concept, the figure of merit of a bipolar transistor is given here:

$$\beta = \frac{I_c}{I_b} = \frac{I_n - I_r}{I_p + I_r + I_s} < \frac{I_c}{I_p} = \beta_{max} \qquad (3\text{-}1)$$

where β_{max} is the possible maximum current gain of a transistor, I_c and I_b are the collector and base currents, respectively. I_n and I_p represent the electron current and hole current components injected across the emitter junction, respectively, and I_r and I_s are the recombination currents within the base region and the space Charge region, respectively. I_n has to increase and/or I_p has to decrease in order to achieve a large current gain. The desire towards the possible maximum current gain β_{max}

leads to the concept of the wide gap emitter.

3.1 Wide–gap Emitter Transistor Concept

The energy diagrams for a homojunction and a heterojunction are drawn in Figure 3.1. For a homojunction, the energy barrier, denoted qV_n, for holes injected from the base into the emitter is the same as the energy barrier, denoted qV_p, for electrons injected from the emitter into the base. Then the current I_n and I_p can be expressed as:

$$I_n = qv_{nb}N_{De}\exp(-qV_n/kT) \qquad (3\text{-}2)$$

and

$$I_p = qv_{pe}N_{Ab}\exp(-qV_p/kT) \qquad (3\text{-}3)$$

where v_{nb} and v_{pe} are the mean speeds of electrons at the emitter–end of the base and of holes at the base–end of the emitter, respectively, and N_{De} and N_{Ab} are the doping concentrations in the emitter and the base, respectively. The ratio of I_n/I_p can be obtained. The ratio is proportional to the ratios of the mean speeds v_{nb}/v_{pe} and the doping levels N_{De}/N_{Ab}. Usually, v_{nb}/v_{pe} is between 5 and 50. Therefore, the doping ratio N_{De}/N_{Ab} is required to be at least 10^2 in order to obtain a useful current gain(e.g. >100). The dependence of the current gain on the doping ratio gives rise to some difficulties to optimize a homojunction transistor. For example, high frequency performance, in turn, low base resistance requires high doping level in the base while high current gain requires low doping level in the base. A possible way to overcome these difficulties is to increase the hole barrier such that the hole current component is much less than the electron current component. This idea can be accomplished by using a wide–gap material for the emitter, implying a hetero-

junction structure.

For a wide–gap emitter heterojunction transistor, the energy barrier holes is at least a few kT larger than the barrier for electrons. The difference between the two barriers is given by:

$$(qV_n - qV_p) = \Delta E_g - \Delta E_b \approx \Delta E_v \qquad (3\text{-}4)$$

Now, the maximum current gain β_{max} is given by [12]:

$$\beta_{max} = \frac{v_{nb}}{v_{pe}} \frac{N_{De}}{N_{Ab}} \exp(\Delta E_v/kT) \qquad (3\text{-}5)$$

Suppose $\Delta E_v = 0.61\Delta E_g = 0.36$ ev(this is the case in InGaAs/InP in which ΔE_g = 0.6 ev). Then, $\exp(\Delta E_v/kT)$ is a factor of 10^6, which is much larger than the mean speed ratio and the doping level ratio. In other words, the maximum current gain is almost only dependent on the valence band discontinuity ΔE_v.

3.2 A Basic Principle of Heterojunction [12]

A basic principle as a guidance in design and development of heterojunction devices simply means that variation of energy gap, resulting in a force acting on carriers, is utilized to control their flows and distributions. This principle can be understood by observing the forces acting on both electrons and holes within a heterojunction device. The forces acting on electrons and holes are equal(but the signs are opposite to each other) to the slopes of the edge of the bands. In a homo-junction, the slopes are supposed to be constant due to the constant energy gap. Therefore, two forces, acting on electrons and holes, are also supposed to be equal

in magnitude and opposite in sign, as shown in Figure 3.2. However, the force acting on electrons is different from that acting on holes in a heterostructure due to the different slopes resulting from the variation of the energy bands, as shown in Figure 3.3.

For example, the idea of the wide–gap emitter originated from the intention that a larger force is added to the holes injected from the base into the emitter than the one to the electrons injected from the emitter into the base. As a result, the ratio of the electron current to the hole current I_n/I_p is increased by the difference, instead of by the difference between the doping levels, between the two acting forces, produced by the different slopes in the conduction band and the valence band. The "spike" at the conduction band is found to have two–fold functions. On one hand, the height of the spike may produce a near ballistic transport through the base, resulting in a high speed. On the other hand, the existence of the spike repels the injection of electrons into the base, leading to a decrease in the ratio I_n/I_p, in turn a decrease in the current gain β. Therefore, an optimum height of the spike is designed to make a compromise according to the device's main requirements.

3.3 Effects of Discontinuities

In fact, the drastic changes caused by HBTs result from the discontinuity of the valence band. The effect of ΔE_v on the current transport can quantitively be expressed by equation (3–5). The physical explanation for this is given in the previous section. Apparently, the possible maximum current gain is uniquely determined by the value of the discontinuity and a very large current gain is abso-

lutely obtainable. Unfortunately, a large value of ΔE_v is not easily achieved. It is affected by the growing processes. The reported values of ΔE_v are good enough to produce successful HBTs.

A brief description of the two–fold functions of the "spike" has been given in the section 3.2. The "spike" results from the conduction band discontinuity ΔE_c. This potential spike project above the conduction band of the narrow gap base, causing a net energy barrier for the injection of electrons from the emitter into the base. If the effect of the carrier transport within the base on the injection is temporally neglected, an extra emitter–base voltage in the order of $\Delta E_b/q$ is required to produce a given electron current density. In other words, the existence of the spike reduces the current ratio I_n/I_p by a factor of $\exp(-\Delta E_b/kT)$. However, the injection of electrons into the base is actually affected by the distribution of the electrons within the base. The extra potential spike may inject the electrons into the base with a substantial kinetic energy such that the electrons move through the base region with a very high velocity($\sim 10^8$ cm/s). Since in III–V compound semiconductors, the dominant scattering mechanism is the polar optical scattering, which is directional dependent, the electrons possess the high forward velocity for several collisions. As a result, a near–ballistic electron transport through the thin base is produced. Such a near–ballistic transport possesses a significant effect on the device speed and the device current gain. It is necessarily noted that an over–high "spike" may result in slow transport velocity because the electrons with high energy will transfer to the next energy valley where the electrons have low mobility. Therefore, the height of the spike needs to be carefully chosen and controlled.

When the spikes, existing at both e–b junction and b–c junction for DHBTs,

become too thin due to the applied voltages, the electrons may tunnel through the spikes. Multi-transport mechanisms have to be considered at the e–b junction since the upper portion of the spike is thin enough to cause the electron tunneling. Tunneling also possibly happens at the b–c junction because of the thin spike caused by the reverse bias. Furthermore, the spike at the b–c junction has repelling effect on the approaching electrons.

3.4 Double Heterojunction Concept [12,15,23]

A Double Heterojunction Bipolar Transistor(DUBT) is the one with wide–gap emitter and wide–gap collector. Its energy diagram is shown in Figure 3.4. Like the use of a wide–gap emitter, the use of a wide–gap collector gives the possibility to optimize the transistor's performances and more design flexibility.

The interchangability between the emitter and the collector is the most important advantage of a DHBT. The performance of the transistor remains the same with the emitter up or down. In other words, The roles of the emitter and the collector can be substituted for each other simply by changing the bias conditions. This feature is significant for highly integrated circuits. For example, an ECL gate has four transistors. The emitters of three transistors are connected to the collector of the fourth. These four transistors can be easily realized by using DHBTs with collector–top configuration within the same insulating island, as illustrated in Figure 3.5.

In the switching digital circuit, the collector is often driven into saturation. Usually, the base region is more heavily doped than the collector. In this case, the

injection of holes from the base into the emitter is severe, resulting in more dissipation and slow speed. For a high switching speed transistor, the suppression of the injection of holes is needed. In DHBTs, the spike introduced by the conduction discontinuity can effectively repel the injection of holes. Therefore, the switching performance is greatly improved if DHBTs are used.

A major drawback of DHBTs is the repelling of the electrons by the second spike at the b–c heterostructure under the reverse bias condition. From the energy diagram, it can be seen that the electrons have to surmount the energy barrier to enter the collector, resulting in a decrease in the collector current I_c. However, this effect decreases with the increase in the reverse bias. This effect will be discussed in more details in the following chapter.

3.5 HBT's Characteristics

As far as a transistor is concerned, I_c-V_{ce} characteristics are typical. Besides this typical characteristic, there actually are more concerns to take into consideration. In many analog applications, a high current gain at very low current density is required. To satisfy this requirement, HBTs are the first qualified candidates. The characteristic of the current gain β versus the collector current I_c important to many applications. β usually varies with the collector current due to the large recombination currents within the space charge region and on the surface around the emitter areas, especially the later is more significant. An InP/InGaAs DHBT with near–ideal β versus I_c characteristic has been reported mainly due to the small surface recombination current in InP, implying a unity emitter injection efficiency [24]. The near–ideal junctions are confirmed by the current–voltage characteristics

of the emitter–base diode and the base–collector diode with junction ideality factor equal to 1, and the characteristic of β versus I_C. As experimental data for the analysis in this thesis, these characteristics of InP/InGaAs/InP DHBT are re–drawn and shown in Figure 3.6.

3.6 Conclusion

The wide–gap emitter concept originated from the concept that injection efficiency can be made independent on the doping levels of both the emitter and the base regions. The possible maximum current gain in a heterojunction transistor is actually dependent on only the valence band discontinuity. This drastic change in transistor design gives rise to the possibility to optimize the transistor's high frequency performance without sacrificing current gain. The conduction band discontinuity plays an important role in carrier injection over the emitter junction and the transport within the base region. A Double Heterojunction Bipolar Transistor(DHBT) can be realized by applying a wide–gap emitter as well as a wide–gap collector. DHBTs produces more design flexibility to optimize the transistor's high speed performance, which is significant in high speed integrated circuit applications.

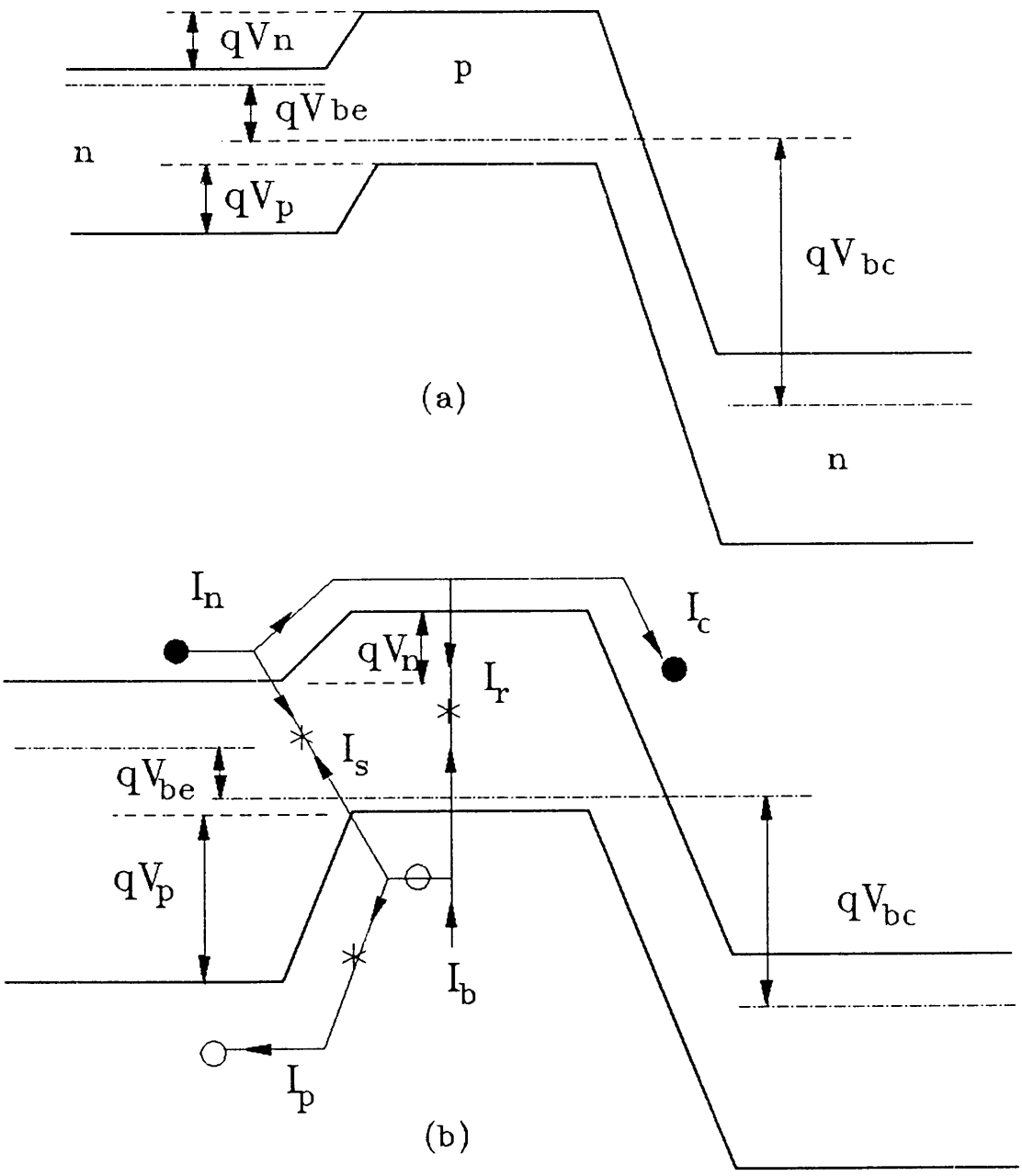

Figure 3.1 Band diagrams of an n p n transistors for (a) homojunction. (b) wide gap emitter, showing current components and the additional hole barrier.

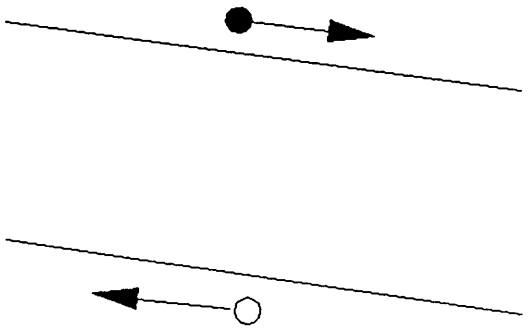

Figure 3.2 Forces acting on electrons and holes in a uniform gap semiconductor

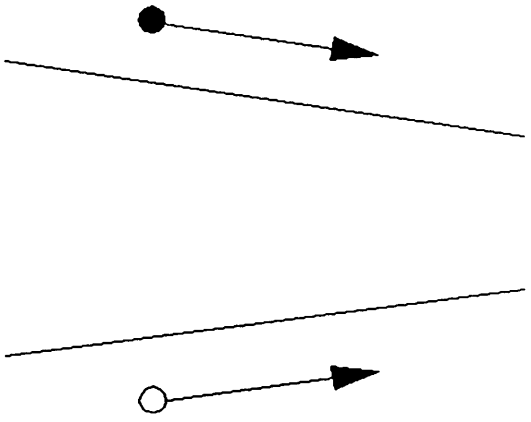

Figure 3.3 Forces acting on electrons and holes in a graded gap semiconductor

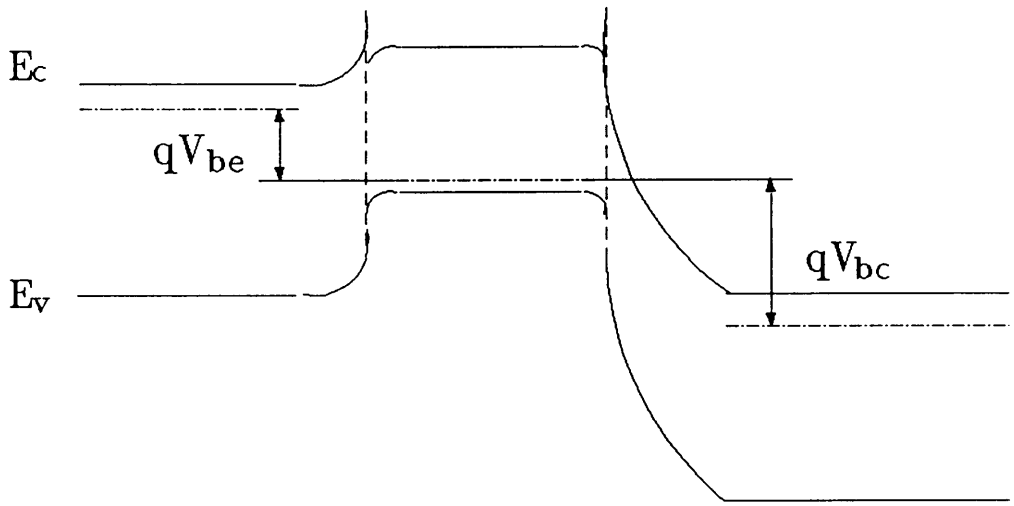

Figure 3.4 Energy band diagram of a DHBT

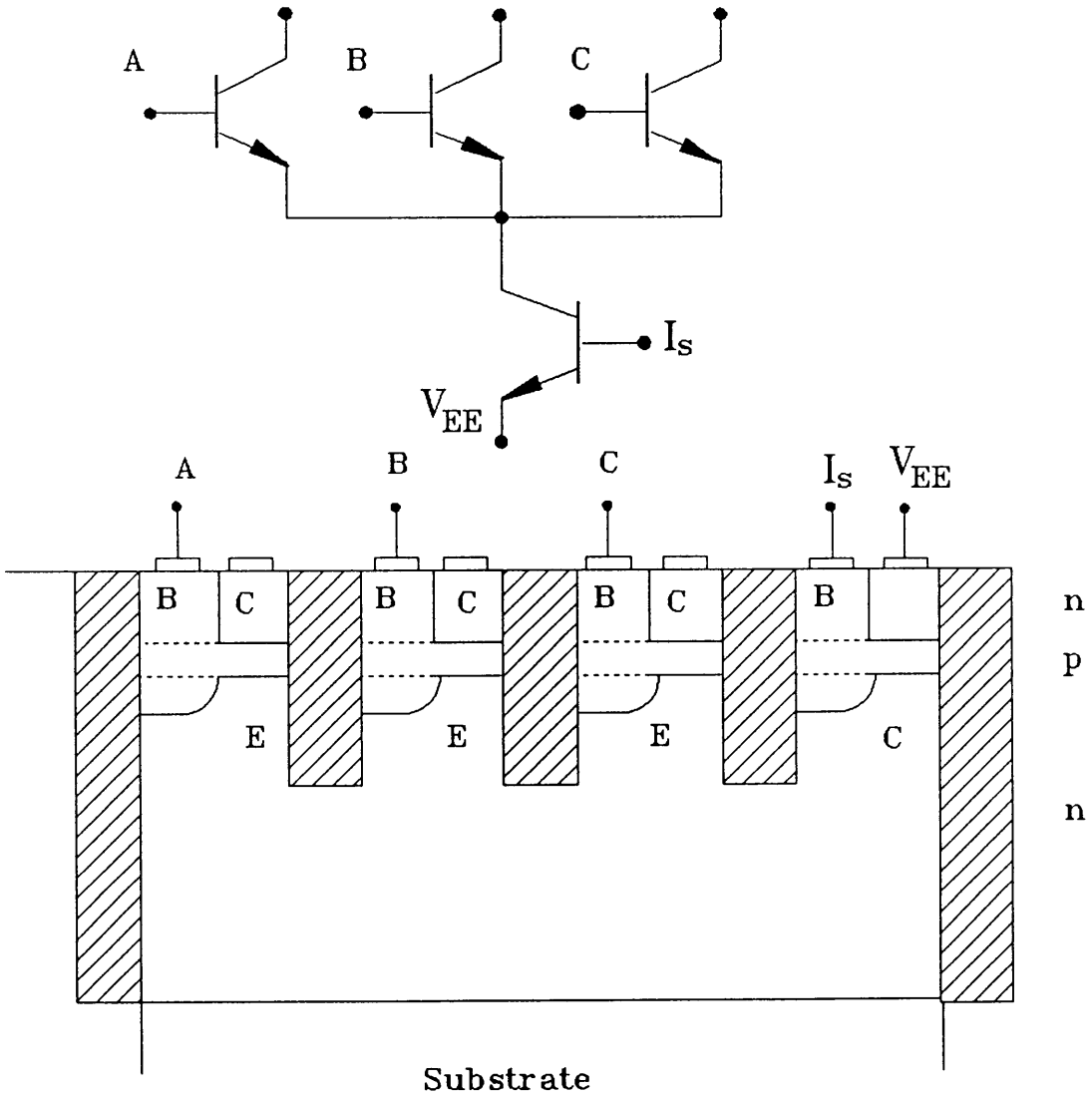

Figure 3.5 An ECL Gate with Double Heterojunction transistor

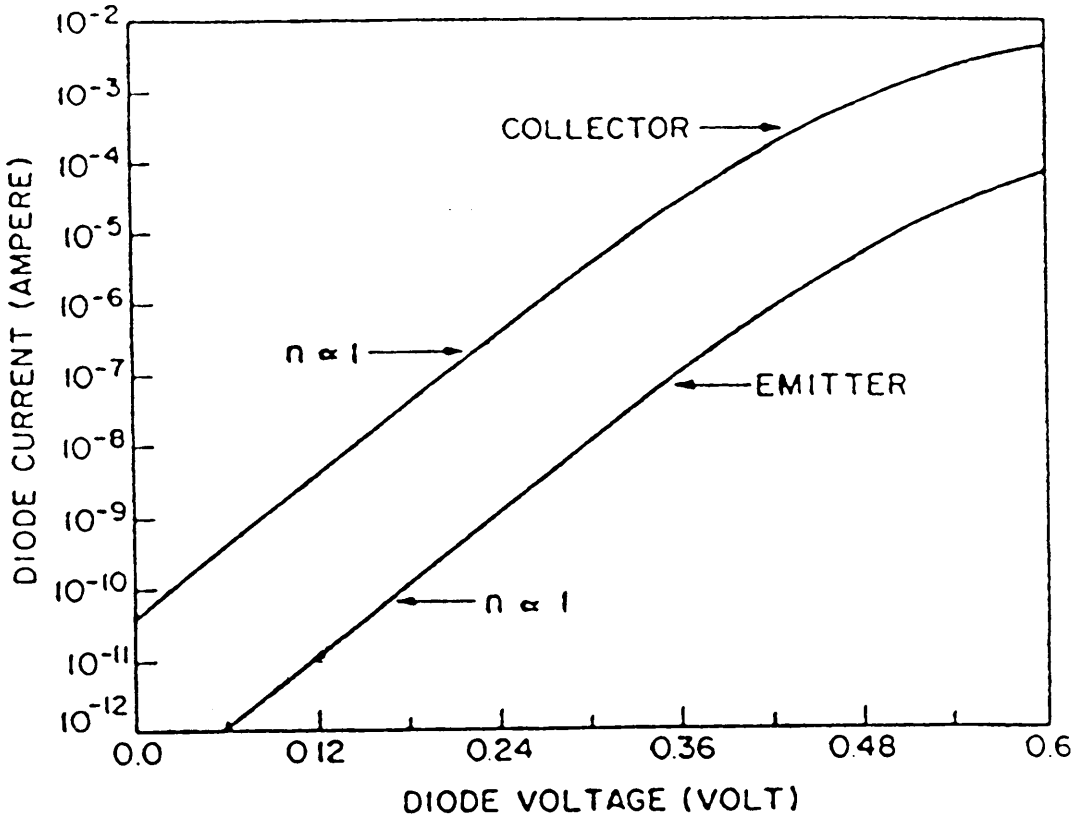

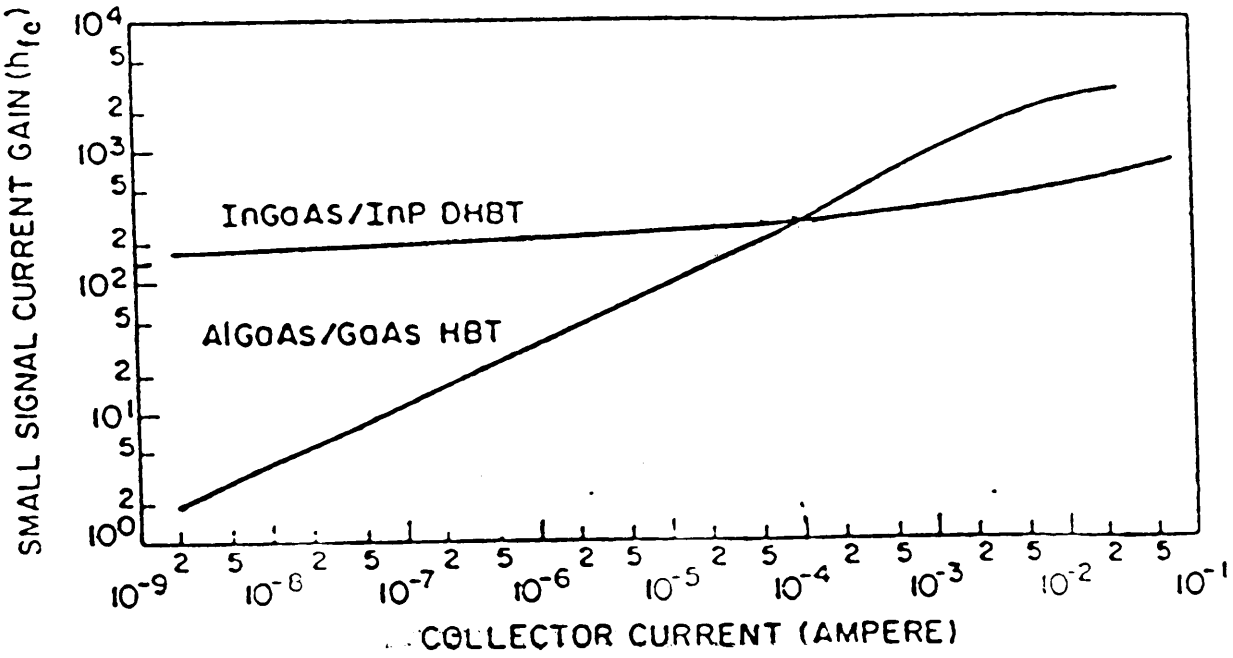

Figure 3.6 I–V characteristics of InGaAs/InP e–b and b–c diodes and β versus I_C for InGaAs/InP DHBT and AlGaAs/GaAs HBT

CHAPTER IV

Theoretical Investigation of Transport Mechanisms For n–p–n InP/InGaAs DHBT

4.0 Introduction

The concerned transport process of injected carriers is accounted for from the edge of the e-b depletion on the emitter side to the edge of the b-c depletion on the collector side. The process consists of the injection of carriers over the e-b junction, the transport through the base, and the collection by the collector. Three theories are used to describe the whole transport process; thermionic emission, drift-diffusion, and tunneling. To order to obtain an accurate current device model, the three current transport mechanisms are applied and the proper boundary conditions are selected, based on the physical considerations, at different boundaries.

InP/InGaAs material system has been proved to be a very promising pair for high frequency transistor applications. The model is applied to a Double Hetero-junction Bipolar transistor. Therefore, the investigation of the current transport processes, discussed in this chapter, is applied to an n–p–n DHBT made from InP/InGaAs/InP.

4.1 Device Physical Structure [25]

The schematic representation of the device structure is illustrated in Figure 4.1. The device can be etched to a mesa configuration to reduce the surface recombination current. A buffer layer is inserted between the InP substrate and the

collector layer. The InP collector region is n–type doped with a concentration equal to $1x10^{17}$ cm^{-3} with a thickness of 0.5 μm. The InGaAs p–type base layer is doped to $2x10^{18}$ cm^{-3} with a thickness of 0.1 μm. The InP emitter layer is then grown on top of the base and doped to $2x10^{17}$ cm^{-3} with a thickness of 0.3 μm. Another layer of heavily–doped InGaAs is formed on top of the InP emitter for metallization contact. The band–gap for InP is 1.35 ev and for InGaAs is 0.75 ev. Therefore, this is a wide–gap emitter and wide–gap collector double heterojunction transistor.

The energy band diagram for the device is illustrated in Figure 4.2. An abrupt heterojunction approximation is taken into consideration. When the biases are applied to the two interfaces, the energy band of the emitter is raised and the energy band of the collector is lowered with respect to the neutral base region. The changes of the energy bands as the biases change are good demonstrations of physical phenomena inside the device, leading to an understanding of carrier transport processes.

4.2 Current Gain β and the Concerned Current Components

The current gain β of the transistor is a good figure of merit to evaluate the performance of the transistor when the description of the carriers transport process is considered. β is given by:

$$\beta = \tau \ \alpha_T \qquad (4-1)$$

where τ is the injection efficiency of the emitter and α_T is the base transport factor.

When the voltages V_{be} and V_{bc} are applied to the e-b junction and c-b

junction, respectively, the four current components, J_n, J_p, J_s, and J_r are included in the whole current transport starting from the edge of the depletion region of the e-b junction on the emitter side, x_1, to the edge of the depletion region of the c-b junction on the base side, x_3. J_n is the electron current density injected from the emitter into the base, J_p is the hole current density injected from the base into the emitter, J_s is the sum of the electron-hole current density due to the generation-recombination within the forward-bias emitter-base depletion region and the surface recombination, and finally J_r is the electron current density of bulk recombination within the base region.

When these four current components are considered, τ, α_T, and β can be expressed in the forms,

$$\tau = \frac{I_n}{I_n + I_p + I_s} \qquad (4\text{-}2a)$$

$$\alpha_T = \frac{I_n - I_s - I_r}{I_n - I_s} \qquad (4\text{-}2b)$$

and

$$\beta = \frac{I_c}{I_b} = \frac{I_n - I_r}{I_p + I_r + I_s} \qquad (4\text{-}2c)$$

where I_c and I_b are the collector terminal current and the base terminal current, respectively.

4.3 Electron Injection Current at e–b Heterojunction (J_n)

For the drift-diffusion current mechanism, the transport current is described

by the Boltzmann transport equation of the form,

$$J_n = q\,\mu_n\,n\,\nabla\phi_n \qquad (4\text{-}3)$$

where ϕ_n is the electron quasi-Fermi level (imref), n refers to the electron concentration, and μ_n is the electron mobility. In the transport equation, two kinds of driving forces associated with electron motion are included; the first force is the imref gradient and the second one is the field. These two forces exist within $x_1 < x < x_j$ without considering the potential energy maximum. When one considers a case where the potential energy barrier is so sharp that electrons one mean free path away from the maximum can gain or lose kinetic energy $\geq kT$, one encounters a serious problem in applying the Boltzmann transport equation properly. The problem is that the field component to the current at the potential energy maximum does not exist anymore. The solution to this problem proposes the use of the thermionic emission [26]. Such a case exists at an abrupt heterojunction due to the conduction band discontinuity ΔE_c at the interface. Therefore, diffusion combined with thermionic emission is considered to treat the electron injection over the energy barrier at the e-b junction.

The basic concept in that solution is that the drift-diffusion is applied within $x_1 < x < x_j$, while the thermionic emission theory is used at the potential energy maximum, actually right at the boundary or the interface.

From equation (4-2), one can obtain,

$$J_n = q\mu_n N_c \exp[-q(\psi_{(x)} - \phi_{n(x)})/kT]\,\nabla\phi_n \qquad (4\text{-}4)$$

where N_c refers to the state density of InP and $\psi_{(x)}$ is the potential distribution within the depletion region. The above equation is integrated between the limits x_1 and x_j, one can obtain,

$$\frac{J_n}{q\ \mu_n\ N_c} \int_{x_1}^{x} \exp[q\psi_{(x)}/kT]dx = \int_{\phi_{n(x1)}}^{\phi_{n(x)}} \exp[q\phi_{n(x)}/kT]\ d\phi_n \qquad (4\text{-}5)$$

If one defines the edge of the depletion region as the reference, equation (4-5) can be obtained,

$$\psi_{(x1)} = \phi_{n(x1)} = 0 \qquad (4\text{-}5)$$

selecting the proper reference and assuming a constant doping concentration, one can obtain from Poisson's equation an expression of the potential distribution of the form,

$$\psi_{(x)} = -qN_{De}(x^2+x_1x)/2\epsilon_1+(1+x/x_1)(V_{bi1}-V_1) \qquad (4\text{-}6)$$

where V_{bi1} and V_1 are the built-in voltage drop and the applied voltage drop, respectively, on the emitter side. Substituting equation (4-6) into (4-4), one can obtain,

$$J_{n(x)} = \frac{\sqrt{2\pi}\ q\ D_n\ N_c\ N_{De}\ \exp[\frac{q\ L_d\ V_1}{2\ x_1\ kT}]^2[\exp(q\phi_{n(x)}/kT) - 1]}{F_{0,1}[(x-k_m)/L_d] - F_{0,1}[-(x_1+k_m)/L_d]} \qquad (4\text{-}7)$$

where L_d is the Debye screen length for an electron concentration equal to the

acceptor doping concentration. L_d is of the form,

$$L_d = \left(\frac{\epsilon_1 \, k \, T}{q^2 \, N_{De}} \right)^{1/2} \qquad (4\text{-}7b)$$

$F_{0,1}(x)$ is the normal distribution function. k_m is a factor of the form,

$$k_m = - \frac{\epsilon_1 \, V_1}{q \, N_{De} x_1} \qquad (4\text{-}7c)$$

Considering thermal emission at the potential energy maximum, one can have [20],

$$J_n = q \, v_{th} \, [\, n_{m(xj)} - n_{0(xj)}] \qquad (4\text{-}8)$$

where v_{th} is the thermal velocity given by equation (4-9),

$$v_{th} = A^* \, T^2 / q \, N_c \qquad (4\text{-}9)$$

$n_{m(xj)}$ is the electron density at x_j when the current is flowing, $n_{0(xj)}$ is a quasi-equilibrium electron density at x_j, and A^* is the effective Richardson constant.

The electron densities $n_{m(xj)}$ and $n_{0(xj)}$ are given by,

$$n_{m(xj)} = N_c \exp\left[- \frac{qV_{bi1} - q\phi_{n(xj)}}{kT} \right] \qquad (4\text{-}10a)$$

and

$$n_{0(xj)} = N_c \exp\left[- \frac{qV_{bi1} - qV_1}{kT} \right] \qquad (4\text{-}10b)$$

Equating equations (4-7), (4-8), and (4-10), one can obtain the expression for electron injection current $J_{d\text{-}t}$ at x_j

$$J_{d\text{-}t(xj)} = \frac{q\, v_{th}\, N_c \exp(-qV_{bi1}/kT)[\exp(qV_1/kT) - 1]}{1 + \dfrac{v_{th}\{F_{0,1}[(x-k_m)/L_d] - F_{0,1}[-(x_1-k_m)/L_d]\}}{\sqrt{2\pi\, D_n L_d \exp[qL_d V_1/(2x_1 kT)]\exp[q(V_1-V_{bi1})/kT]}}} \qquad (4\text{-}11)$$

In addition to the diffusion and the thermionic emission mechanisms, it is possible for electrons to tunnel through the energy barrier due to the energy-band structure. From Figure 4.2, it can be seen that part of the "spike" at the e-b hetero-junction is above the conduction band of the base. This portion increases as the applied voltage increases. In other words, those electrons on the emitter side with energy less than the height of the "spike", Eb, but larger than the energy level of the base conduction band, may form a current by tunneling through the "spike". In fact, this is the case where tunneling occurs from one conduction band into another conduction band. To evaluate the tunneling current J_{tun}, one can have [27,28],

$$J_{tun} = \frac{4\pi q m^*}{h^3} \int dE\{F_{e(E)} - F_{b(E)}\} \int P_{(Ex)}\, dE_x \qquad (4\text{-}12)$$

where E_x is the electron energy in the tunneling direction, $F_{e(E)}$ and $F_{b(E)}$ are the Fermi-Dirac distribution functions in the emitter conduction region and the base conduction region, respectively, and $P_{(Ex)}$ is the tunneling probability given by,

$$\ln P_{(Ex)} = -\alpha \int (\psi_{(x)} - E_x)^{1/2} \, dx \qquad (4\text{-}13)$$

$$\alpha = 2 (2m^*)^{1/2}/h$$

It is very difficult to obtain an accurate analytical expression for $P_{(Ex)}$ from equation (4-13) for the given potential expression $\psi_{(x)}$. However, equation (4-13) can be evaluated by expanding it with respect to a carefully-chosen energy level E_t. By selecting a certain E_t means that electrons with energy close to E_t have large tunneling probability. Then, $P_{(Ex)}$ can be expressed as

$$\ln P_{(Ex)} = -[\, a + b(E_t - E_x) + \cdots] \qquad (4\text{-}14)$$

where,
$$a = \alpha \int_{x_{11}}^{x_{12}} [\psi_{(x)} - E_t]^{1/2} \, dx$$

$$b = 1/2 \, \alpha \int_{x_{11}}^{x_{12}} [\psi_{(x)} - E_t]^{-1/2} \, dx$$

and $(x_{11} - x_{12})$ is the tunneling length.

4.4 The Recombination current In The Base Region (J_r)

The injected carriers from the emitter into the base are considered to diffuse through the neutral base region. The bulk recombination current forms during the diffusion. According to the diffusion theory, the diffusion current can be determined as long as the excess electron distribution is obtained. The magnitude of the recombination current is equal to the subtraction of two currents $J_n(x_2)$ and $J_n(x_3)$ at the two boundaries of the base, respectively.

In order to obtain the excess electron distribution $\Delta n_p(x)$ within the base

region, the continuity equation is solved in the one-dimensional case under steady-state conditions,

$$D_{nb} \frac{d^2 \Delta n_p(x)}{dx^2} - \frac{\Delta n_p(x)}{\tau_{nb}} = 0 \qquad (4\text{-}15)$$

where D_{nb} and τ_{nb} are the electron diffusion coefficient and the electron lifetime in the base region, respectively.

As seen from the energy band diagram, the "spike" due to the conduction band discontinuity plays an important role in affecting further transport of injected electrons after crossing it. In fact, the "spike" may inject the electrons into the base region with a substantial kinetic energy, and hence with a very high velocity [12]. The kinetic energy results from the transformation of the potential energy concerning the height of the spike. Estimation of the electron velocity when electrons "fall" down from the top of the spike may be made using a simple expression of the form,

$$1/2\ m^*\ v^2(x) = \Delta E_n \qquad (4\text{-}16)$$

and,

$$\Delta E_n = \Delta E_c - q(\ V_{bi2} - V_2\ ) \qquad (4\text{-}17)$$

where v is the initial velocity with which electrons move away from the interface, m^* is the electron effective mass, ΔE_c is the conduction band discontinuity, ΔE_n is the potential energy of the spike, V_{bi2} and V_2 are the built-in voltage drop and the applied voltage drop on the base side. Since all the injected electrons move initially with high velocity in a positive direction away from the interface, the Boltzmann Statistics, requiring the random distribution of the velocity, is not satisfied[28]. Only

when the injected electrons experience several periods of scattering, the traditional diffusion equation can be applied. Usually, the mean free path of an electron between collisions is of the order of 10^2 Å. The calculated value of the width of the depletion region on the base side is less than 10^{-6} cm. Thus, one can reasonably assume that the injected electrons reach the edge of the neutral base region almost without loss. In other words, the concentration of the excess electrons which begin to diffuse at $x = x_2$ across the base region is the same as the amount of the injected electrons at $x = x_j$. According to the above statement, the excess electron concentration is given by,

$$\Delta n_p(x_2) = J_n(x_j)/[q\ v(x_j)] \qquad (4\text{-}18a)$$

The influence of the excess electron level by the e-b junction applied voltage V_{be} is through J_n for V_1 and v for V_2.

Taking the effect of the spike at b-c junction into consideration (will be discussed in the next section), one can find the boundary condition at $x = x_3$ of the form,

$$\Delta n_p(x_3) = J_n(x_3)/qv_t \qquad (4\text{-}18b)$$

where v_t is the transport velocity at the boundary $x = x_3$.

Based on the two boundary conditions, equations (4-18a) and (4-18b), the excess carrier distribution is obtained,

$$\Delta n_p(x) = \frac{1}{\sinh(W_b/L_{nb})}[\Delta n_p(x_2)\sinh(\frac{W_b - x}{L_{nb}}) + \Delta n_p(x_3)\sinh(x/L_{nb})] \quad (4\text{-}19)$$

Then, an expression for J_r can be derived as,

$$J_r = J_n(x_2) - J_n(x_3)$$

$$= \frac{q\ D_{nb}\ \Delta n_p(x_2)}{L_{nb}}[\frac{\cosh(W_b/L_{nb})}{\sinh(W_b/L_{nb})} - \frac{1}{A}(\frac{B}{\sinh^2(W_b/L_{nb})}) - \frac{1}{A\ \sinh(W_b/L_{nb}}] \quad (4\text{-}20)$$

where,

$$A = B\ \frac{\cosh(W_b/L_{nb})}{\sinh(W_b/L_{nb})} + 1$$

$$B = \frac{D_{nb}}{v_t\ L_{nb}}$$

$L_{nb} = (D_{nb}\,\tau_{nb})^{1/2}$ is the electron diffusion length, τ_{nb} and D_{nb} are the electron lifetime and the electron diffusion coefficient, respectively, within the base region.

4.5 Effect of the b–c Barrier on the Transport Process

The injected electrons encounter the second spike at the b-c junction. It is assumed that they reach that boundary, $x = x_3$, with the thermal velocity $V_{th}/4$ [29]. Two possibilities exist for them to cross this barrier into the collector region; one is that the electrons penetrate through the barrier by tunneling. This case occurs usually with a low reverse bias at which the barrier is high but thin. When a high

reverse bias is applied so that the height of the barrier decreases further more and even disappears, the thermal emission of the carriers across the barrier can be possible. The electron blocking action of the spike causes the injected electrons to be accumulated more and consequently more recombination is expected. This leads to a decrease in β and dependence on V_{ce} as well. The effect of the spike on the electron transport can be described in terms of a transport velocity v_t, which is an exponential factor less than the thermal velocity $v_{th}/4$. For the tunneling case[30],

$$v_t = v_{th}/4 \exp[-2(2m^*/\hbar^2)^{1/2} \Delta E_o^{1/2} d] \qquad (4\text{-}21)$$

For the thermal emission case, v_t may be written as,

$$v_t = \frac{v_{th}}{4} \exp(-\frac{\Delta E_o}{kT}) \qquad (4\text{-}22)$$

where $\hbar$ is the reduced Plank's constant, d is the thickness through which the electrons tunnel, and ΔE_o is the height of the barrier given by,

$$\Delta E_o = \Delta E_c - q(V_{bi2} - V'_2) \qquad (4\text{-}23)$$

V'_2 is the voltage drop of the applied bias at the base region side. It is noticed that a simplified expression for tunneling current, instead of equation (4-12), is used due to the reverse-biased junction. Obviously, v_t is a function of V_{bc} since the features of the energy barrier is determined by V_{bc}.

4.6. The Recombination Current In Depletion Region (J_s)

An expression for the bulk recombination current $I_{rg,b}$ for the heterojunction

under consideration is derived as,

$$J_{rg,b} = q \left[\int_0^{x_1} U_1 \, dx + \int_0^{x_2} U_2 \, dx \right] \qquad (4\text{-}24)$$

where U_1 and U_2 are the recombination rates within x_1 and x_2, respectively. U_1 and U_2 are given by,

$$U_1 = (1/2)\, \sigma_1\, v_{th1}\, N_{t1}\, n_{i1}\, \exp(qV_1/2kT) \qquad (4\text{-}25)$$

$$U_2 = (1/2)\, \sigma_2\, v_{th2}\, N_{t2}\, n_{i2}\, \exp(qV_2/2kT) \qquad (4\text{-}26)$$

where σ_1, σ_2, v_{th1},v_{th2}, N_{t1}, N_{t2}, n_{i1}, and n_{i2} are defined in the Table 1.

On the other hand, the surface recombination current is given by,

$$I_{rg,s} = (1/2)\, q\, n_{i2}\, s_0\, A_s \exp(qV_{be}/2kT) \qquad (4\text{-}27)$$

where s_0 is the surface recombination velocity, A_s is the base surface area where recombination occurs. s_0 is of the form,

$$s_0 = \sigma_2\, v_{th2}\, (\pi\, k\, T\, D_{st}) \qquad (4\text{-}28)$$

Thus, J_s can be represented as,

$$J_s = J_{rg,b} + J_{rg,s} \qquad (4\text{-}29)$$

4.7. Hole Injection Current at e-b Heterojunction (J_p)

It is known that the hole current component is greatly suppressed by the valence band discontinuity ΔE_v. The ratio of the electron injection current J_n to the

hole injection current J_p is approximately evaluated by equation (3-1), rewritten as,

$$J_n/J_p = \beta_{max} = A \exp(\Delta E_v/kT) \qquad (4\text{-}30)$$

where A is a constant and ΔE_v is the valence band discontinuity between InP and InGaAs. Since ΔE_v is about ten times of kT for the material system considered, the ratio is at least larger than 10^3. Practically, J_p is much less than the recombination current J_s, or $J_p << J_s$. This simply means that the hole current component J_p becomes negligible compared to the recombination current. Therefore, it is not necessary to evaluate J_p in detail in this study.

4.8 Simulation Results and Analysis

Computations of these current components are based on the material parameters recently reported for InGaAs and InP in the literature and structural parameters of the device shown in Figure 4.1. The material parameters are given in Table 1. The diffusion-thermionic emission and the tunneling current components are evaluated first. The result of $J_{d\text{-}t}$ is presented in Figure 4.3. The current density value at V_{be} = .8 v is about 10^4 amps./cm^2. Different values of E_t, which are $0 < E_t < E_b$, are used to compute the tunneling currents J_{tun}. The results are shown in Figure 4.4, indicating that E_t = .5 E_b possesses the largest tunneling probability value. Comparing the results of Figure 4.3 and Figure 4.4, one can find that the diffusion-thermionic emission current dominates over the tunneling current component by a factor of 10^2. The reason can be mainly attributed to the barrier's thickness. As known, the tunneling current is quite sensitive to the energy barrier's thickness. A thickness of the energy barrier for a doping concentration of 2 x 10^{17}/cm^3 is about 500 Å, which is not thin enough to cause a significant tunneling

current. However, if the thickness is decreased by increasing the doping concentration, the tunneling current component increases rapidly. The computation of the tunneling current versus doping concentrations is shown in Figure 4.5. One can observe that the tunneling current is dominant as the doping concentration exceeds $5x10^{17}/cm^3$. The diffusion-thermionic emission and the tunneling components can be distinguished by observing their slopes in current-voltage (I-V) characteristics. The latter possesses a greater slope than the former. This is due to the fact that the tunneling current is a strong function of the applied voltage through both the energy of the electrons and the thickness of the energy barrier. Therefore, the dominant injection mechanism varies with the applied voltage range and the doping concentration of the device.

Figure 4.6 illustrates the current gain β and Figure 4.7 presents the injection efficiency γ and the transport factor α_T in the base region. An emitter area of about 10^{-6} cm^2 is used to compute the current gain. It can be seen that the current gain β over the range of the current from 10^{-1} to 10^{-6} Amperes. is almost constant. This result is in good agreement with the experimental result reported in reference [24]. The reason for the excellent β characteristics is mainly attributed to the great reduction of the recombination current. The low recombination current at the InP-InGaAs interface is due to the excellent lattice match of these two materials. The results also indicate that the magnitude of the current gain β are strongly affected by different values of the ratio of the base width to the diffusion length. Actually, this ratio determines the magnitude of the transport factor α_T, in turn β, when the injection efficiency γ is quite close to one. The ratio is related to the values within the parenthesis in the expression for J_r. If the diffusion length in such an extremely thin base layer is chosen as 1.3 μm [31,32], the corresponding β would be

as high as 10^3. This mainly results from the very short base width and very high carrier velocity of the injected electrons to transit across the base region in such a device structure. A thin base layer without buffer between the InGaAs layer and the InP layer has a very short minority carrier lifetime due to the presence of lattice strain and high density traps. However, the injected electrons go through it only experiencing a few times of scattering when the thickness of the base region is made comparable to the carrier mean free path, which is of the order of one hundred Å.

The value of the transport velocities at the second "spike" is determined in terms of the barrier height, the width of the second spike, and the energy that the electrons possess. The barrier height varies with the doping levels at both the base and the collector regions, as well as with the applied voltage. The results show that when the difference in doping level between the two regions is less than 10^1, the barrier disappears as the voltage V_{bc} greater than 2 volts is applied. Therefore, it is not necessary to consider its effect on the carriers transport. However, if the difference reaches 10^2 or larger, the electron blocking action occurring at the second spike is significant. Figure 4.8 demonstrates that the transport velocities for both cases are quite low at low voltage range. As the applied voltage increases, the tunneling transport velocity increases rapidly and eventually reaches the thermal velocity $v_{th}/4$, indicating that the tunneling transport is dominant at the high voltage range. This is mainly due to the decrease of the barrier height and the increase of the relative energy of the electrons. For low voltage range, the electron blocking action at the second spike can be eliminated by keeping small difference in doping levels between the two regions.

4.9 Conclusion

The injection mechanisms of electrons from the emitter into the base can be described by the diffusion, the thermionic emission, and the tunneling theories. It is important to consider the potential distribution of the energy barrier, especially at the maximum point, in applying appropriately the diffusion and the thermionic emission theories. The tunneling current component can be significant for the injection current at the e-b interface when the doping concentration in the emitter region is larger than $5x10^{17}/cm^3$. The first "spike" at the conduction band discontinuity plays an important role in initiating the injected electrons to enter the base region with a very high velocity. The electron blocking action of the second "spike" at the b-c junction at low voltage range can be eliminated by keeping a small difference in doping level between the base and the emitter regions. Since many physical factors, which affect the transport process of the injected carriers, are taken into consideration, the model obtained in this paper is more complete for n-p-n InP/InGaAs abrupt DHBTs. The methods and the results are also useful and helpful for further theoretical and experimental studies in the future.

Table 1: Material Parameters Used In The Computations. [33-36]

Parameter	Symbol	Value
InP bandgap	E_{g1}	1.35 eV
InGaAs bandgap	E_{g2}	0.75 eV
Conduction band discontinuity	ΔE_c	0.20 eV
Valence band discontinuity	ΔE_v	0.38 eV
InP effective electron mass	m^*_{n1}	0.077 m_0
InGaAs effective electron mass	m^*_{n2}	0.034 m_0
InP permittivity	ϵ_1	12.8 ϵ_0
InGaAs permittivity	ϵ_2	11.7 ϵ_0
InP intrinsic carrier concentration	n_{i1}	$10^7/cm^3$
InGaAs intrinsic carrier concentration	n_{i2}	1.2×10^{12} cm^{-3}
InP thermal velocity	v_{th1}	4.23×10^7 cm/s
InGaAs thermal velocity	v_{th2}	6.37×10^7 cm/s
InP capture cross section	σ_1	7×10^{-16} cm^2
InGaAs capture cross section	σ_2	3×10^{-17} cm^2
InP capture center density	N_{t1}	3×10^{16} cm^{-3}
InGaAs capture center density	N_{t2}	1.5×10^{13} cm^{-3}
Electron diffusion const in base region	D_n	2.85×10^2 cm^2/s
Hole diffusion const in emitter region	D_p	3.75×10 cm^2/s
Eff. state den. in cond. band of InP	N_{c1}	4.16×10^{17} cm^{-3}
Eff. state den. in val. band of InGaAs	N_{v2}	1.37×10^{19} cm^{-3}
State den. of surface recomb of III-V	D_{st}	8×10^{-11} $cm^{-2}eV$

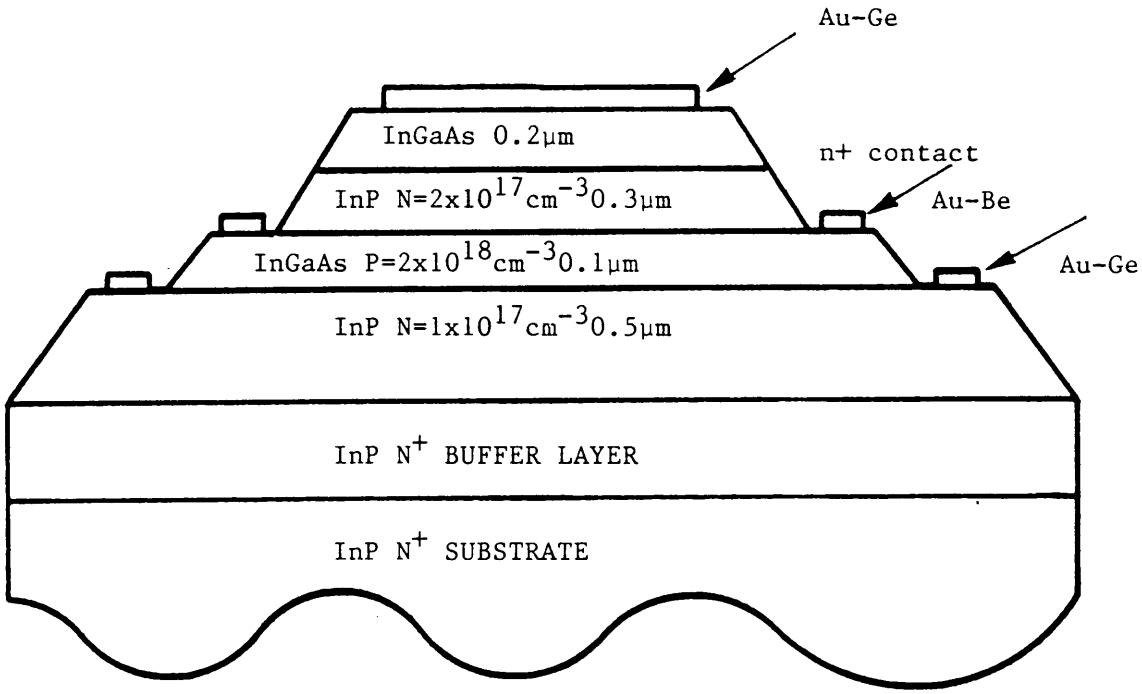

Figure 4.1 Schematic representation of the device structure of a n–p–n InP/InGaAs/InP DHBT

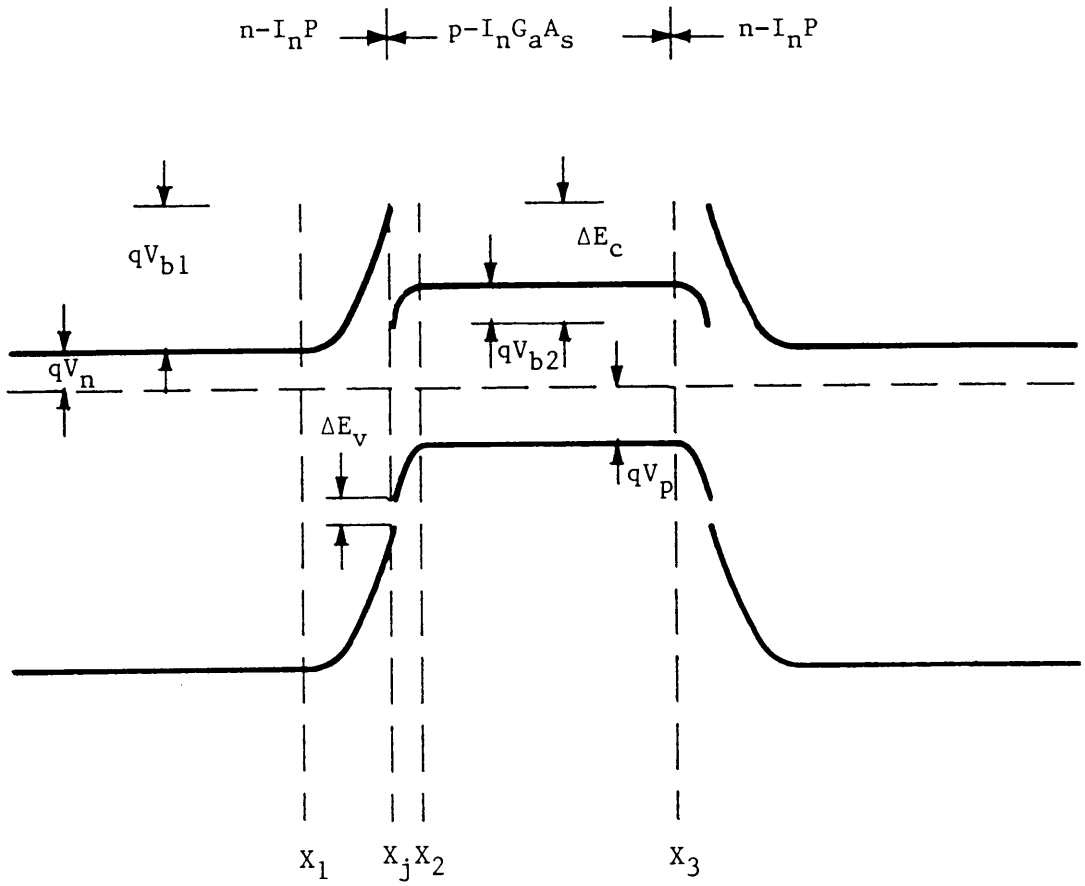

Figure 4.2 The energy band diagram for n–p–n InP/InGaAs/InP DHBT

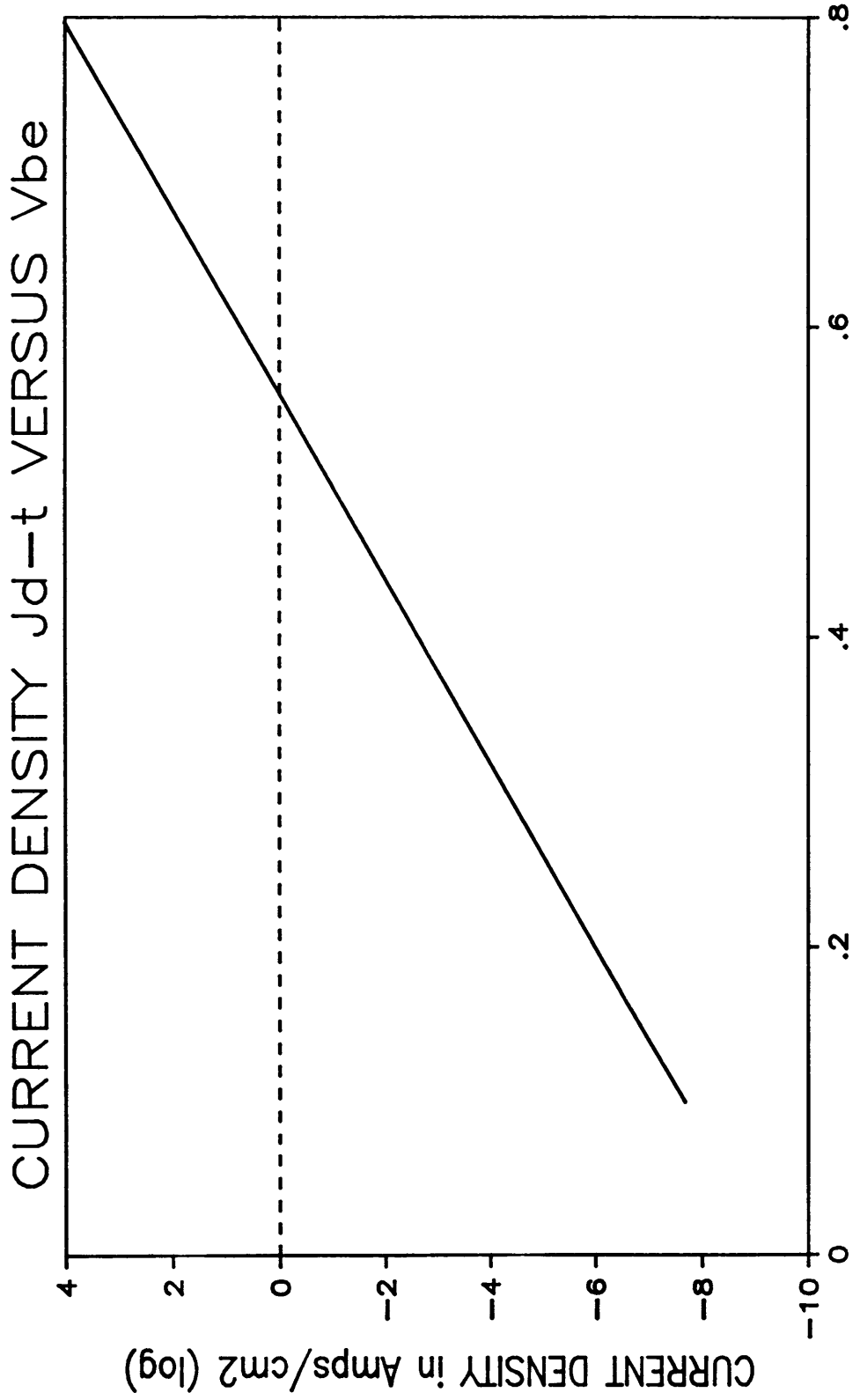

Figure 4.3 The diffusion–thermionic current component versus V_{be}

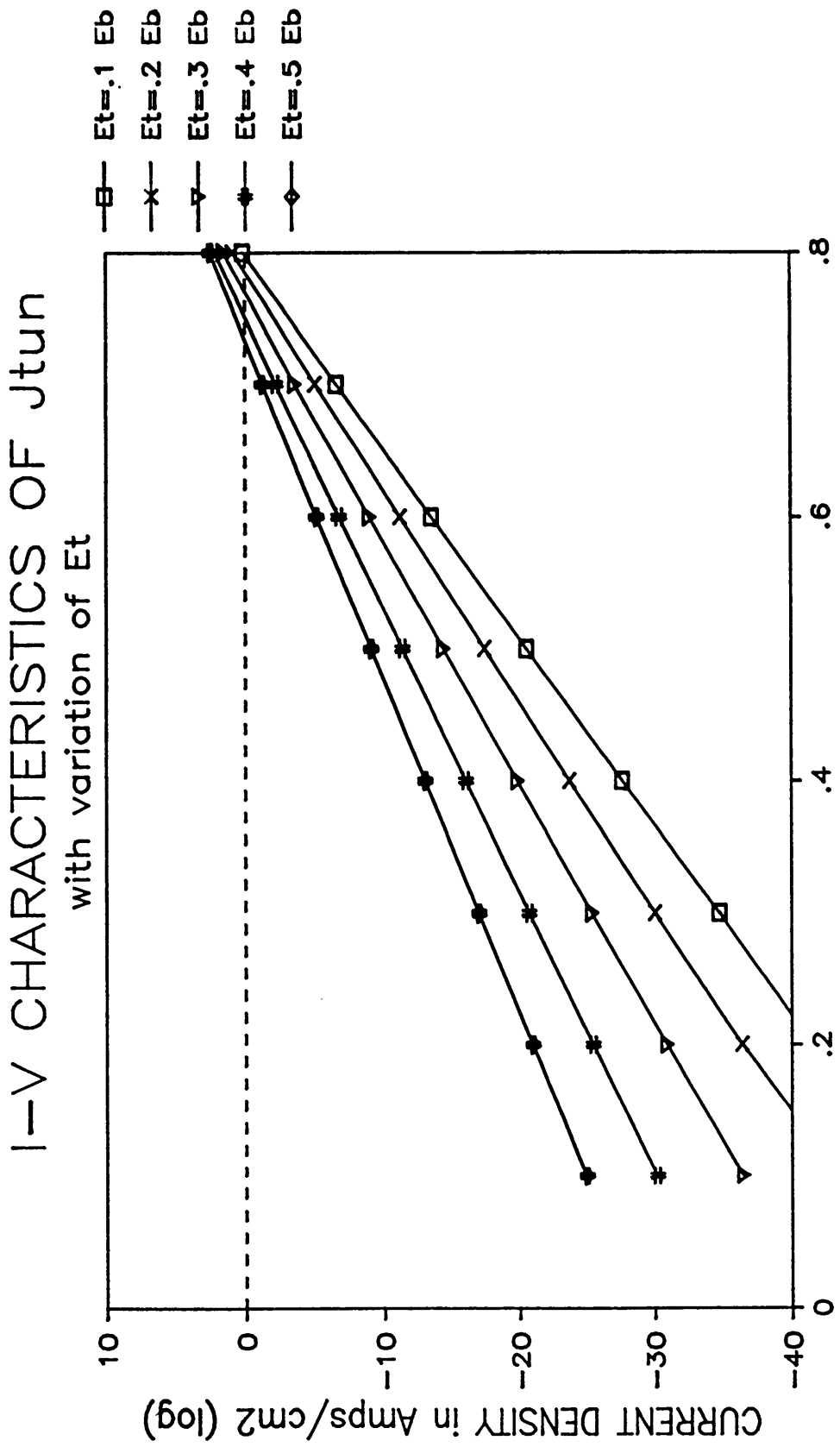

Figure 4.4 The tunneling current component versus V_{be} with variation of energy level E_t

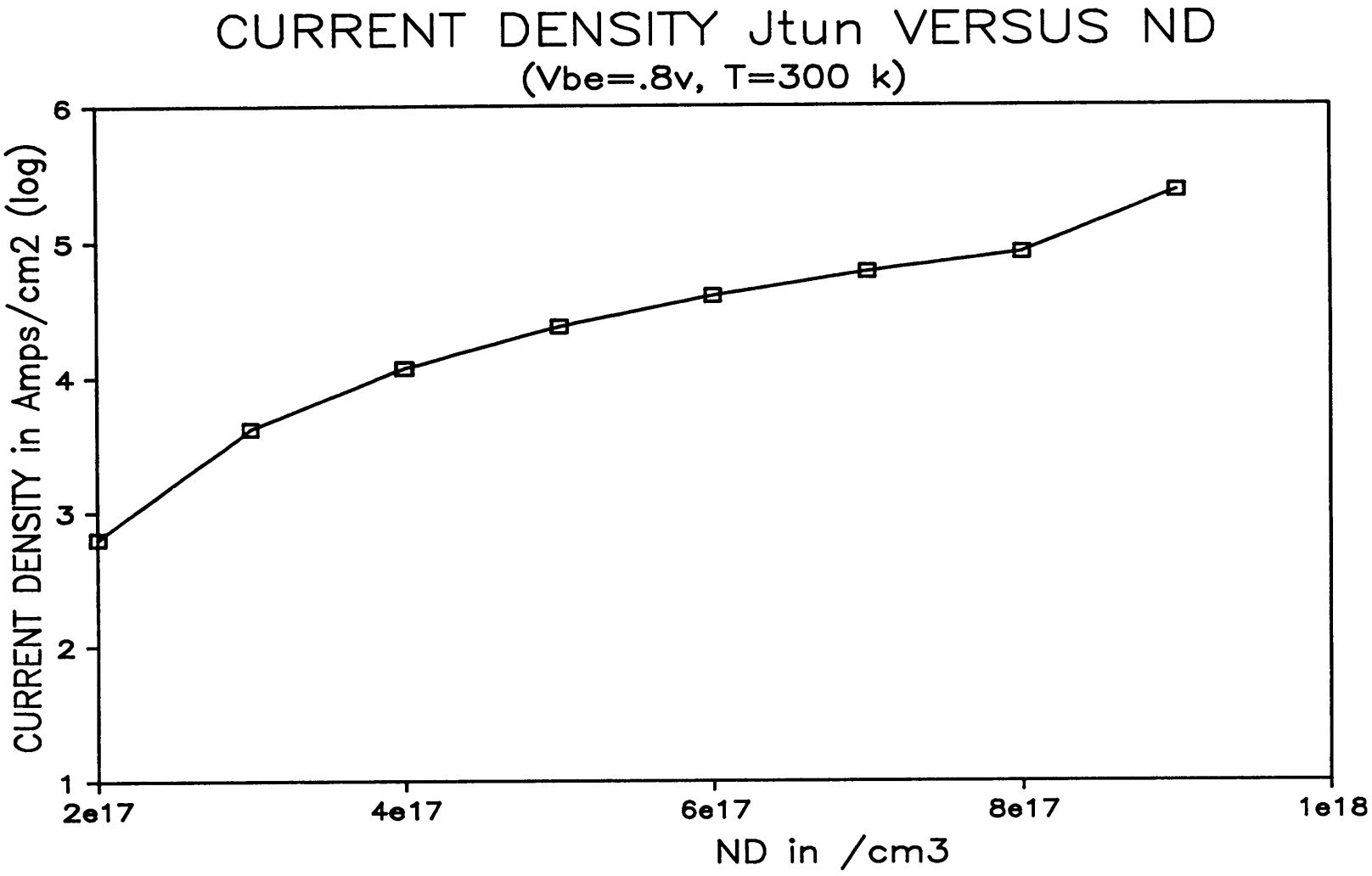

Figure 4.5 Tunneling current component versus doping concentrations.

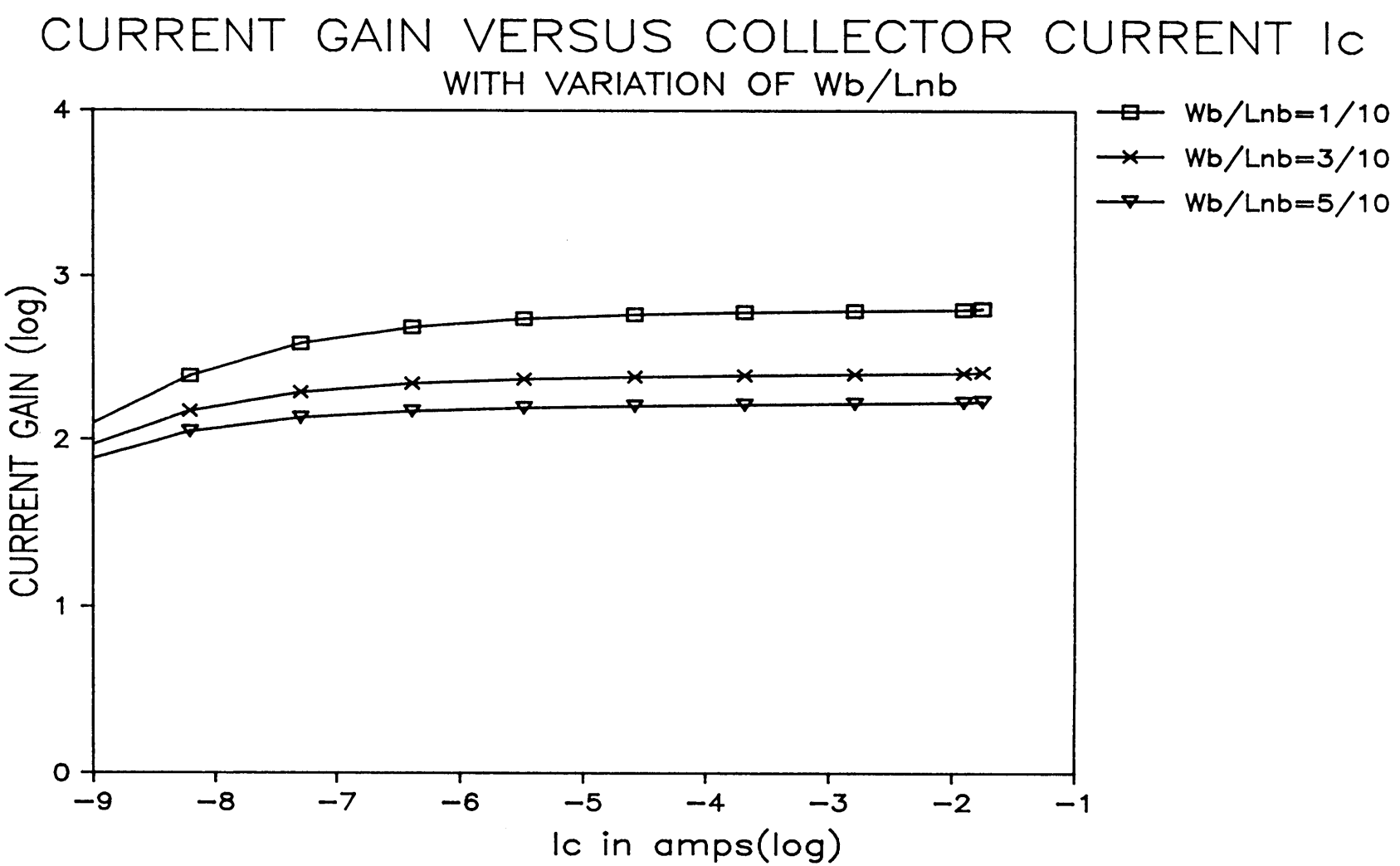

Figure 4.6 The current gain β versus the collector current I_c with variation of W_b and L_{nb}

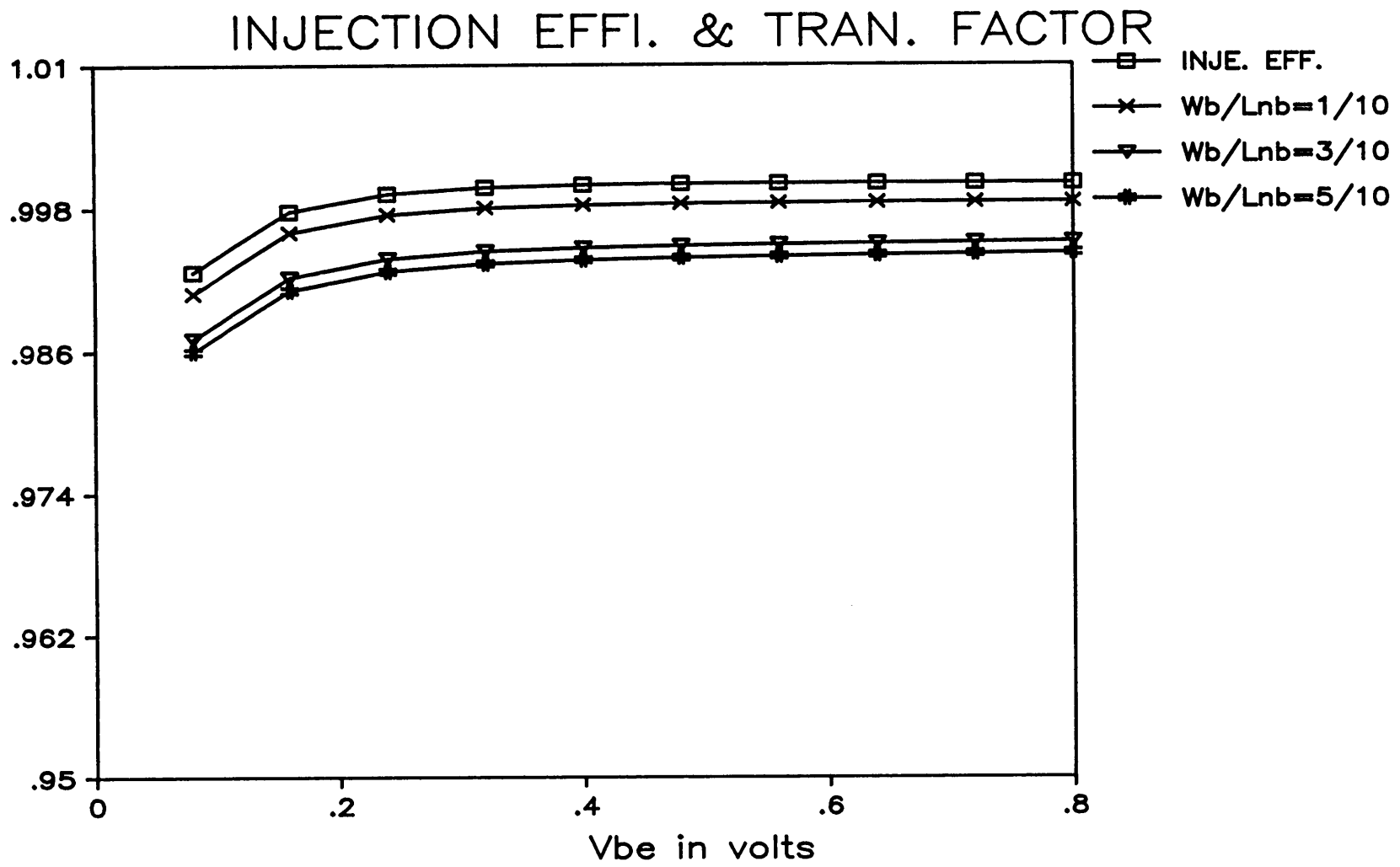

Figure 4.7 Injection efficiency & transport factor versus V_{be}

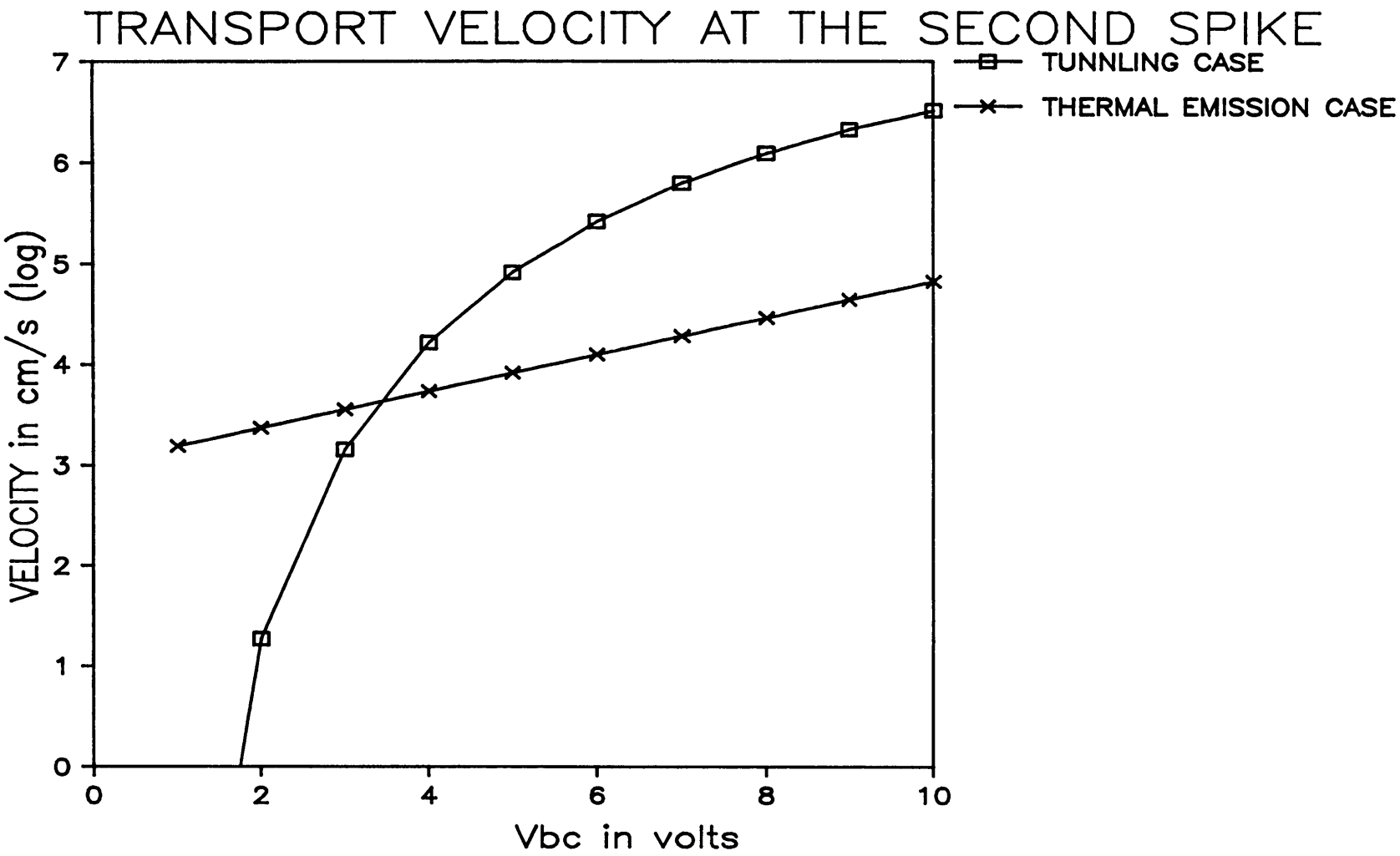

Figure 4.8 Transport velocities at b–c heterojunction versus V_{bc} for tunneling and thermionic cases

CHAPTER V

Considerations in Microwave Applications

5.0 Introduction

In practical applications, the requirement of bipolar transistor's high current gains is not the main interest. Except some special cases, a β value of around 100 is good enough. Therefore, the significant benefit from HBTs is its ability to optimize its performances at higher level. The most important performance that is to be optimized is the one at high frequency or at microwave frequency.

It is author's intention to conduct research, as continuation of the present work, on application of microwave techniques to characterize HBTs in future. To serve as this purpose, a brief survey of special considerations of HBTs in microwave applications is given.

5.1 General Requirements of performance at High Frequency

The cutoff frequency f_T is an important figure of merit for a microwave transistor. f_T is defined as the frequency at which the common emitter short–circuit current gain $h_{fe}(=\partial I_c/\partial I_b)$ is unity. Actually, f_T describes the ability to possess current gain at high frequency. It is well known that β value is frequency–dependent. β decreases as frequency increases. This dependence is due to various effects of capacitance and resistance through the whole transport process. These effects can be described as RC charging–discharging process. β value is determined by the lost portion of the injected carriers from the emitter. The more

injected carriers lost, the less the β value. The lost injected carriers due to the increase in frequency are considered as the contribution to the discharging current of RC effects. Obviously, higher frequency results in larger discharging current, leading to the decrease in β. Therefore, microwave transistor is required to have current gain at high frequency, implying high f_T.

Another important figure of merit is the maximum oscillation frequency f_{max}, which is defined as the frequency at which unilateral gain becomes unity. The unilateral gain is the forward power gain in a feedback amplifier with its reverse power gain set to zero. Therefore, f_{max} describes the performance of the power gain of the transistor at high frequency. Sometimes, f_{max} is called the unity power gain frequency while f_T is called unity current gain frequency. Since the output impedance of a transistor is higher than the input impedance, the transistor can still possess the ability of power amplification even at the condition when the current gain is unity. For a microwave transistor, it is needed to deliver power output to the load. Therefore, the transistor is required to have power gain at high frequency, implying high f_{max}.

Noise figure is another important figure of merit for microwave transistors. The noise figure is the ratio of total mean–square noise voltage at the output of the transistor to mean–square noise voltage at the output resulting from thermal noise in source resistance. It is understandable to require the transistor to have small noise figure. The noise figure is of great concern at high frequency as compared to lower frequency case since the noise figure increases approximately as f^2.

5.2 Transit Time τ Evaluation

As mentioned above, f_T is the one of the important figures of merit of HBTs at high frequency. The cutoff frequency f_T is related to the physical structure of the transistor through the emitter–to–collector delay time, or the transit time τ by:

$$f_T = \frac{1}{2 \pi \tau} \tag{5-1}$$

The transit time is actually the sum of four delays encountered sequentially by the carriers as they flow from the emitter to the collector [23]:

$$\tau = \tau_e + \tau_b + \tau_c + \tau'_c \tag{5-2}$$

where:

τ_e is the emitter transit time. τ_e is of the form,

$$\tau_e = r_e(C_e + C_c)$$

$$= kT/qI_e(C_e + C_c) \tag{5-3}$$

τ_b is the base transit time. τ_b is of the form,

$$\tau_b = W_b^2/2D_n \tag{5-4}$$

τ_c is the collector depletion transit time. τ_c is of the form,

$$\tau_c = x_{bc}/2v_{sat} \tag{5-5}$$

τ'_c is the collector region transit time. τ'_c is given by,

$$\tau'_c = r_c C_c \qquad (5\text{-}6)$$

where $r_e = kT/qI_e$ is the emitter resistance, C_e and C_c are the emitter capacitance and collector capacitance, respectively, x_{bc} is the depletion width of the b–c junction, v_{sat} is the field drift saturation velocity, and r_c is the collector series resistance.

The maximum oscillation frequency f_{max}, as expected, is related to both the cutoff frequency and the RC constant of the combination base resistance–collector capacitance. f_{max} is of the form,

$$f_{max} = \frac{1}{4\pi} (\omega_T / r_{bb'} C_c)^{1/2} \qquad (5\text{-}7)$$

where $\omega_T = 2\pi f_T$ and $r_{bb'}$ is the base transverse resistance. Although a question about the accuracy of equation (5-7) is raised recently [36,37], the equation does not lose its significance in analyzing high frequency ferformance of transistors due to its intuitive expresion.

When HBTs are used as switching transistors, the switching time τ_s is the parameter to describe the transit process. The switching time τ_s is given by:

$$\tau_s = \frac{5}{2} r_{bb'} C_c + \frac{r_{bb'}}{r_c} \tau_b + (3C_c + C_L) R_L \qquad (5\text{-}8)$$

where C_L and C_L are the load resistance and the load capacitance, respectively.

From the view of the design considerations, most of the requirements of the

physical structure of the device are the same to all these figures of merit of microwave transistors and high speed transistors. However, individual of these figures needs to be considered when the performance of the transistor is optimized. Considerations in optimization will be discussed later.

5.3 Special Device Design Considerations [12,23,25]

The general design considerations of microwave transistors can be classified into two aspects: the reduction of the device dimensions and the selection of materials and configuration. At the present time, advanced technologies have made it possible to reduce the horizontal dimension to submicron and the vertical dimension to a few hundred angstrons. For HBTs, special considerations should be taken in the selection of the material parameters and the device configuration.

1. For a microwave transistor, the main interest is the high frequency output power, or the increase in f_{max}. The increase in the base doping actually results in two benefits. One is the great reduction of the base resistance r'_{bb}, which in turn causes an increase in f_{max}, according to equation (5-7). The second benefit is that the reduction of the base resistance leads to a high current density capability, which improves the tradeoff between speed and power of the wicrowave transistor. The limitations to the increase in the base doping comes from two aspects: the technological constraints and the need to keep the minority lifetime in the base above 10^{-10}s.

2. Besides the base resistance, the increase in the base doping also results in the optimization of the emitter capacitance. Since the heterojunction permits the independence of β on both the base doping and the emitter doping, a drop in emitter

doping is possible. For a highly unsymmetrically doped p–n junction, it is well known that the capacitance is considered to be only a function of the lightly doped level. When the emitter doping drops below the base doping, the emitter capacitance can be represented in the form:

$$C_e \propto N_{De}^{1/2} \tag{5-9}$$

Obviously, a significant reduction can be obtained when the emitter doping is greatly dropped. From equations (5-1) - (5-3) and equation (5-7), the reduction of emitter capacitance causes an increase in the cutoff frequency and, in turn, makes improvement of microwave performance. Also, the reduction of the emitter capacitance leads to great reduction of the noise. The limitations to the lowest emitter doping are the effect of the series emitter resistance and the crystal achievable low purity.

3. The base resistance actually consists of two parts: the inner base resistance and the outer base resistance. The inner base resistance is the portion underneath the emitter, while the outer base resistance is the portion between the edge of the emitter and the base contacts. The heavily doped base reduces greatly the inner resistance, as discussed above. The significance of the outer base resistance depends on the device configurations. For a heterojunction transistor, the geometry can be made like the one shown in Figure 5.1. In this configuration, the wide–gap emitter is constructed as an island, in which the outer base resistance is greatly minimized. A similar configuration is the mesa configuration, which is shown in Figure 5.2. However, these configurations result in difficulties encountered in the manufacturing technology, and as a result the realization cost is higher. To avoid the extra

effort to minimize the outer base resistance, an alternative configuration is the one with the wide–gap emitter extended beyond the emitter edge, forming a part of the base which is a p–n homojunction. This configuration is shown in Figure 5.3. This configuration, actually being similar to homojunction bipolar transistor, can be easily realized. The wide–gap layer with relatively low n–type is first grown as the emitter. The part outside the emitter is then heavily p–type doped to form wide–gap base. The energy diagram for this wide–gap emitter–base homojunction is shown in Figure 5.4, in which it can be seen that the injection current through this wide–gap portion is negligible, compared to the wide–narrow portion, due to the extra barrier of ΔE_g.

4. The concept of the emitter–base junction can be made as wide–gap junction which does not affect the injection current density gives rise to the inverted collector configuration, shown in Figure 5.5. In this inverted transistor, the emitter has a larger area than the collector. In other words, the collector can be made much smaller area, implying a significantly small collector capacitance. Practically, the reduction of the collector capacitance C_c has more significant effects of improving the high frequency performance. These beneficial effects can be recognized by analyzing equation (5-1) — (5-8).

5.4 Construction of Network Model

More and more computer software packages have been developed to aid the microwave characterization techniques. For example, Touchstone[39], developed by EEsof, features a variety of simulation of RF/microwave designs and measurements. It possesses a list of RF devices, transmission lines, and lumped elements models.

Simulation of S-parameters for two-port or four-port models gives rise to the evaluation of microwave performance of these models in the frequency domain. MTCAP(Modified Transient Circuit Analysis Package), developed by the Time Domain Laboratory at Virginia Tech [40], is designed for simulation of microwave circuit's transient performance in the time domain. With Time Domain Reflectometry, an iteration technique can be used to obtain microwave device models. Based on knowledge of physical nature of the device to be modeled and the results of measurements, the configuration of the device using both lumped and distributed circuit elements is to be devised. Then, computer-fitting results in an accurate model, which can be used to compute the microwave parameters of the device and to design microwave circuit.

The first step which is involved in characterization of microwave devices is to understand the structure of the devices and their physical nature. Usually, terminal parameters of the devices can be measured. However, some physical parameters, which are used to describe internal physics of the devices, are not easily known. Although it is difficult to accurately relate the physical models to the electronic models of the devices, it is necessary to possess knowledge of physical models of the devices and related parameters before attempting to characterize the devices. Models developed under the condition of DC and/or low frequency are considered to be the basis on which microwave models are to be developed. Effects occurring at microwave frequencies are added by introducing lumped and distributed elements. These effects then can be evaluated and modeled by measuring the characteristics of the devices, such as S-parameters and impulse response.

The essential operation in HBT is that the current collected by the output

terminal collector is controlled by the base current. This process is modeled into a current-controlled current source. The transit process for electrons within the base region can be modeled into resistors and capacitors, or RC discharging circuits. Various parasitic effects on the transistor can be modeled by resistance, capacitance, and inductance. Based on these considerations and the device structure, a lumped element equivalent circuit for the HBT is proposed and shown in Figure 5.6 [41].

The values of the lumped elements in the proposed electronic model is initially evaluated and given by physical model of the device. Computer simulation of the electronic model with the given values is carried out. At the same time, microwave measurements, conducted in the time domain and the frequency domain, of the device are performed. Then, the simulated result and the experimental result are compared. The values of the lumped elements need to be adjusted to fit the simulated results to the measured results, producing a final electronic model with proper values of the lumped elements.

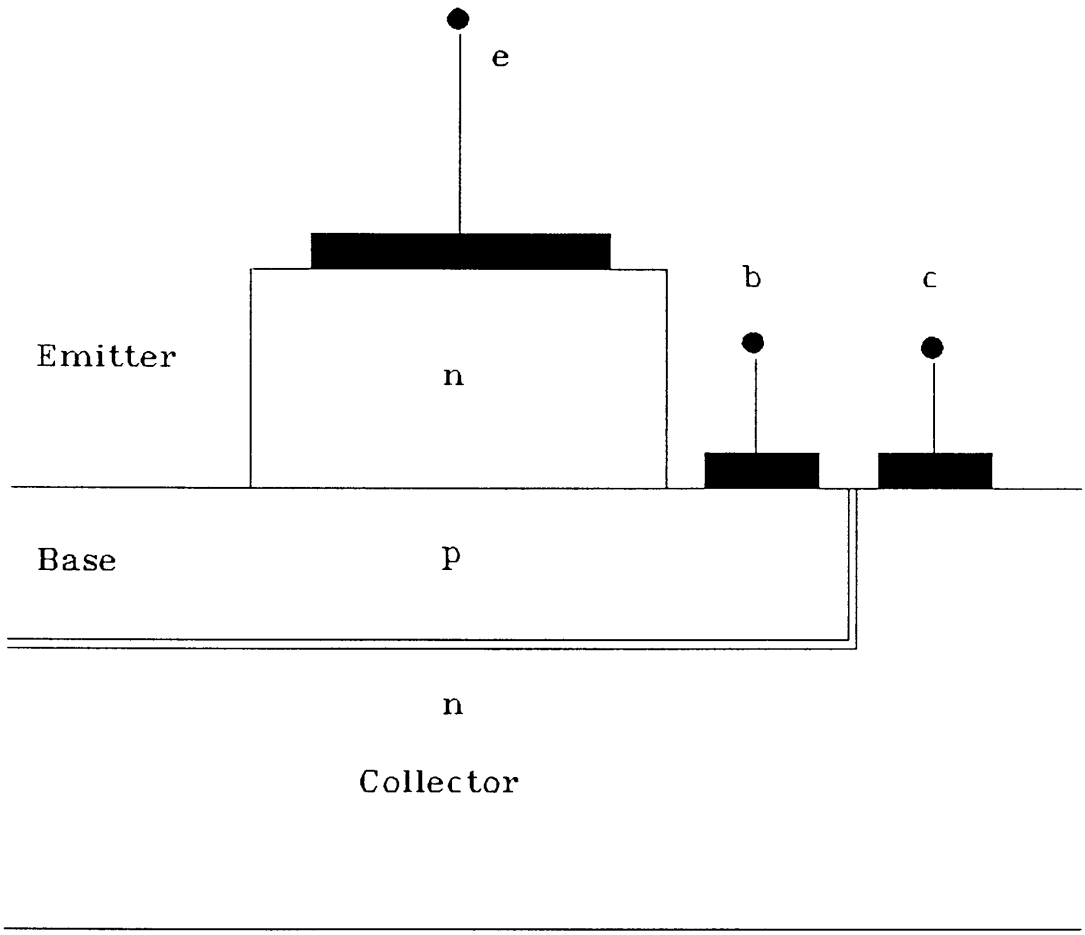

Figure 5.1 A HBT Structure with an Emitter Island

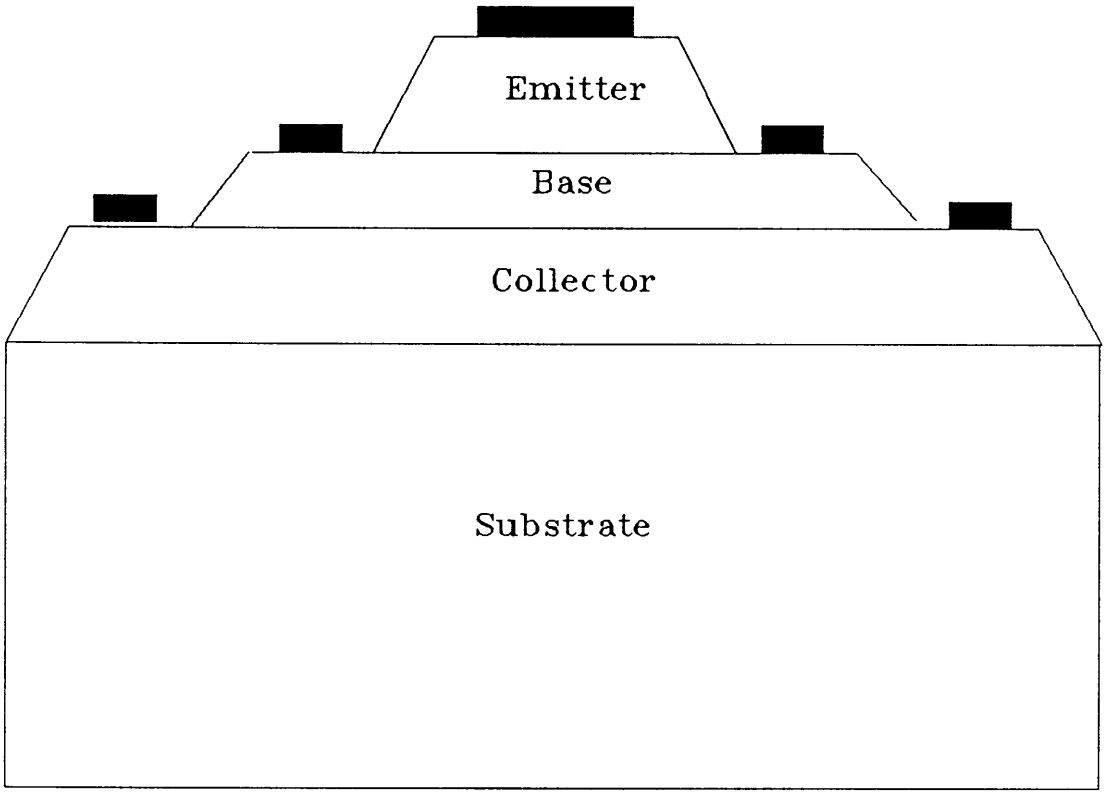

Figure 5.2 A HBT structure with a Mesa Configuration

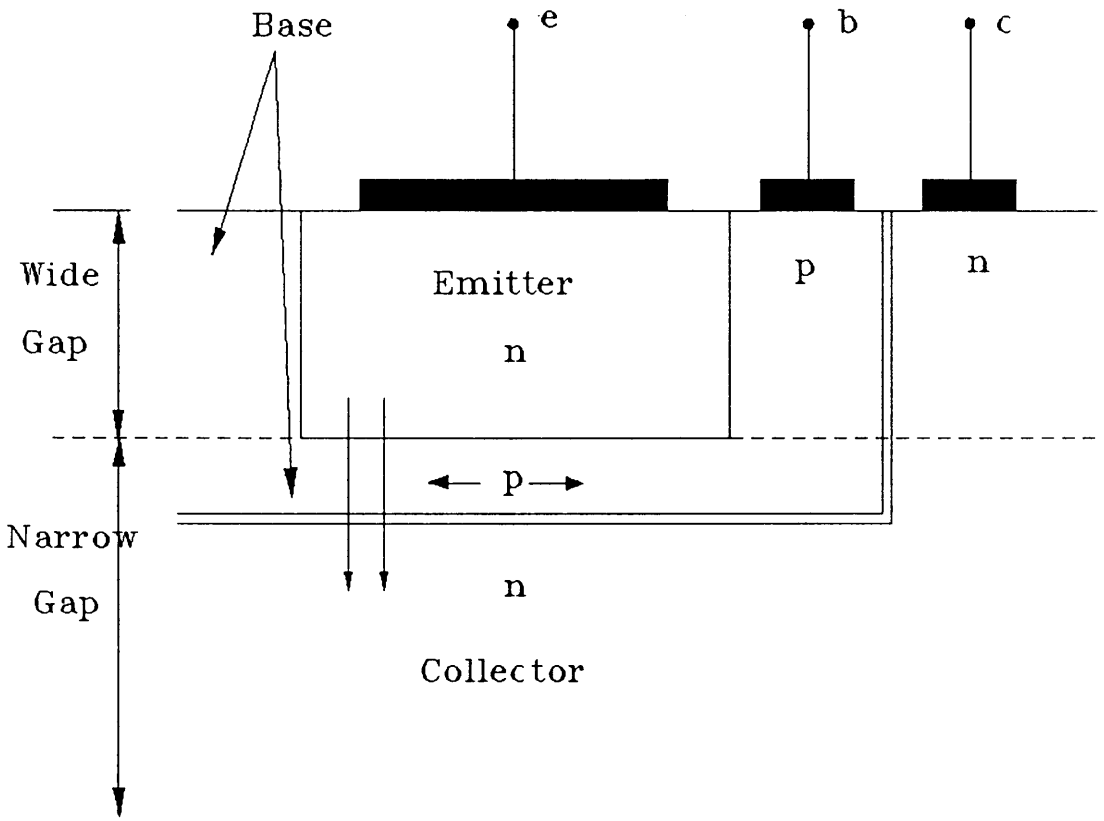

Figure 5.3 An Emitter Structure with a Wide Gap Base, Forming a p–n Homojunction.

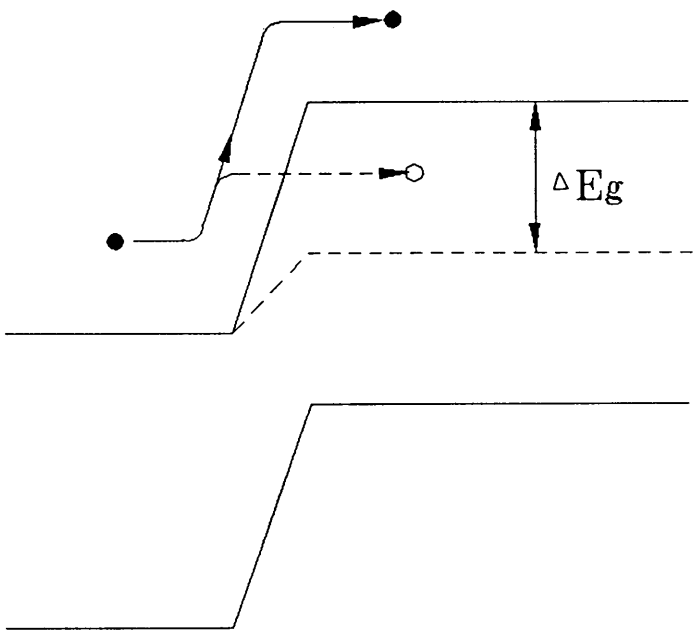

Figure 5.4 The Energy Diagram Showing the Blocking of Injection of Electrons into Wide Gap Base.

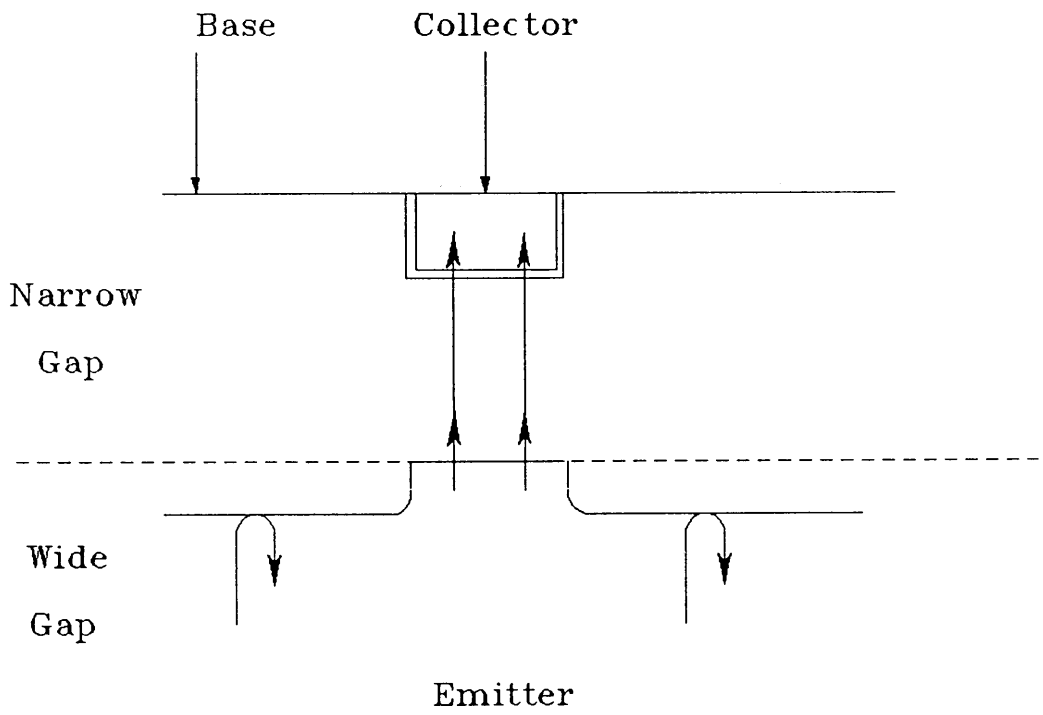

Figure 5.5 Inverted collector–up HBT structure with a larger emitter area, but the no injection of electrons in the external emitter

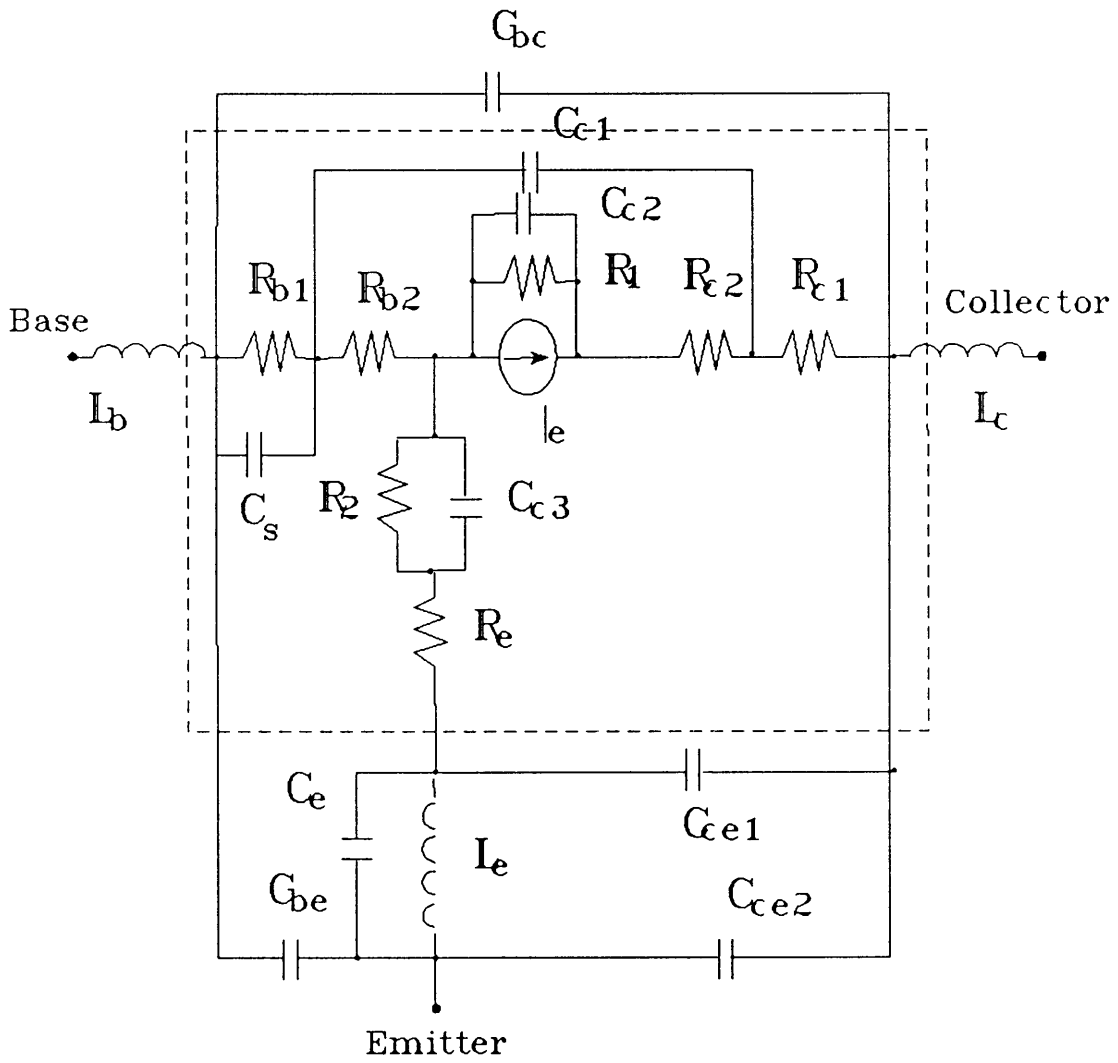

Figure 5.6 A lumped element equivalent circuit of a HBT

CHAPTER VI

Conclusion and Future Directions

Based on the fundamental knowledge of Heterojunction Bipolar Transistors(HBT) provided in the first three chapters, a thorough investigation of mechanisms of carrier injection and transport for an HBT is conducted. The following conclusions are derived:

1. The injection mechanisms of electrons from the emitter into the base can be described by the diffusion, the thermionic emission, and the tunneling theories. It is very important to consider the potential distribution of the energy barrier, especially at the point of the maximum, in applying appropriately the diffusion and the thermionic emission theories.

2. The tunneling current component can be significant for the injection current at the e-b heterointerface when the doping concentration in the emitter region is larger than $5x10^{17}/cm^3$. In such a case, the tunneling current component should be taken into consideration in order to accurately describe the current injection at the e-b junction.

3. The first "spike" at the conduction band at the e-b heterointerface plays an important role in initiating the injected electrons to enter the base region with a very high velocity. This launching action greatly reduces the electrons transit time as well as provide a proper boundary condition for the solution of non-equilibrium carrier distribution, which essentially determines the carrier transport within the base region.

4. There is an electron blocking action at the second "spike" at the b-c hetero-junction. This blocking action becomes insignificant as the reverse voltage increases. At low voltage range, this blocking action can be eliminated by keeping a small difference in doping level between the base and the emitter regions.

5.The physical model obtained is more complete for n-p-n InP/InGaAs/InP abrupt DHBTs since many physical factors that affect the carrier transport are taken into consideration. Therefore, the model provide the future research on HBTs with a fundamental basis.

As suggested in Chapter V, the following topics are considered to be suitable for future research:

1. Extend the obtained one-dimensional model to two-dimensional case , where more practical simulations are needed.

2. Relate the physical model to an electrical network model, which consists of electrical lumped elements.

3. After the network model with lumped elements is set up, microwave characterization techniques are applied to evaluate the high frequency performance of these devices.

4. Develop techniques, both theoretical and experimental, for characterization of HBTs in microwave frequency.

BIBLIOGRAPHY

1. R.M. Kolbas, N.G. Anderson, W.D. Laidig, Yongkun Sin, Y.C. Lo, K.Y. Hsieh, and Y.J. Yang, " Strained-Layer InGaAs-GaAs-AlGaAs Photopumped and Current Injection Lasers." IEEE J. Quantum Electronics,Vol. 24, No. 8, p 1605, August 1988.

2. A. Furuya, M. Makiuchi, O. Wada, and T. Fujii, " AlGaAs/GaAs Lateral Current Injection Multiquantum Well (LCI-MQW) Laser Using Impurity-Induced Disordering," IEEE J. Quantum Electronics, Vol. 24, No. 12, p2448, December 1988.

3. D. Wake, L.C. Blank, R.H. Walling, and I.D. Henning, " Top-Illuminated InGaAs/InP p-i-n Photodiodes with a 3-dB Bandwidth in Excess of 26 GHz," IEEE Electron Device Letters, Vol.EDL-9, No.5, pp.226 - 228, May 1988.

4 H. Hulu and H. Morkoc, " Modulation-doped FETs and Other High Speed III-V Transistor," SPIE, Vol. 795, pp.12 - 28, 1987.

5. W. Schockley, U.S. Patent 2,569,347 (1951).

6. H. Kroemer, " Theory of a Wide-gap Emitter for Transistors," Proc. IRE, Vol. 45, p 1535, 1957.

7. S.R. McAfee, D.V. Lang, and W.T. Tsang, " Observation of Deep Levels Asscoci-

ated with the GaAs/$Al_xGa_{1-x}As$ Interface Grown by Molecular Beam Epitaxy," Appl. Phys. Letters, Vol. 40, No. 6, p 520, 1982.

8. R.N. Nottenburg, H. Temkin, M.B. Panish, and R.A. Hamm, " High Gain InGaAs/InP Heterostructure Bipolar Transistor Grown by Gas Source Molecular Beam Epitaxy," Appl. Phys. Letters, Vol. 49, No. 17, pp. 1112 - 1114, October 27, 1986.

9. R.N. Nottenburg, Y.K. Chen, M.B. Panish, D.A. Humphrey, and R. Hamm, " Hot-Electron InGaAS/InP Heterostructure Bipolar Transistors with f_T of 110 GHz," IEEE Electron Device Letters, Vol. EDL-10, No. 1, pp. 30 - 32, January 1989.

10. K. Tomizawa, Y. Awano, and N. Hashizume, "Monte Carlo Simulation of AlGaAs/GaAs Heterojunction Bipolar Transistors," IEEE Electron Device Letters, Vol. EDL-5, No. 9, p 362, September 1984.

11. K. Tomizawa, Y. Awano, N. Hashizame, and M. Kawashima, " Simulation of Near Ballistic Electron Transport in a Submicron GaAs Diode with $Al_xGa_{1-x}As$/GaAs Heterojunction Cathod," IEE Proc. 132, Pt. 1, No. 1, p 37, 1985.

12. H. Kroemer, " Heterostructure Bipolar Transistors and Integrated Circuits," Proc. IEEE, Vol. 70, No. 1, January 1982.

13. H. Kroemer, " Heterostructure, Bipolar Transistors: What Should We Build? ," J.

Vaccum Science Technology, Vol B1, No. 1, pp 126 - 130, June 1983.

14. J.L. Peloward, R. Castegne, and P. Hesto, " Monte Carlo Study of Ballistic Transport in Heterojunction Bipolar Transistors (DHBJTs) and in High Electron MObility Transistors (HEMTs) ," SPIE, Vol. 795, 1987.

15. J.P. Bailbe, A.Marty, and G. Rey, " III-V Heterojunction Bipolar Transistors," Solid State Electronics, Vol. 30, No. 11, pp. 1159 - 1169, 1987.

16. A.G. Milnes, " Heterojunctions: Some Knowns and Unknowns," Solid State Electronics, Vol. 30, No. 11, pp. 1099 - 1105, 1987.

17. A.A. Grinberg, M.S. Shur, R.J. Fischer, and H. Morkoc, "An Investigation of the Effect of Graded Layers and Tunneling on the Performance of AlGaAs/GaAs Heterojunction Bipolar Transistors," IEEE Transactions On Electron Devices, Vol. ED-31, No. 12, pp. 1758-1765, December 1984.

18. S.C. Lee, J.N. Kau, and H.H. Lin, "Current Transport Across the Emitter-Base Potential Spike in AlGaAs/GaAs Heterojunction Bipolar Transistors," J. Appl. Phys., Vol. 58, No. 2, pp. 890-895, July 1985.

19. A.G. Milnes, "Semiconductor Heterojunction Topics: Introduction And Overview," Solid-State Electronics, Vol. 29, No. 2, pp. 99-121, 1986.

20. S.M. Sze, "Physics of Semiconductor Devices," John Wiley & Son, Chapter 5, pp245-263, 1981.

21. A.G. Milnes and D.L. Feucht, " Heterojunctions and Metal-Semiconductor Junctions," Academic Press, New York and London, 1972.

22. Y.G. Chai, C. Yuen, and G.A. Zdasiuk, "Investigation of $In_{0.53}Ga_{0.47}As$ for High-Frequency Microwave Power FET's," IEEE Transaction on Electron Devices, Vol. ED-32, No. 5, pp. 972-977, May 1985.

23. S.R. Forrest, P.H. Schmidt, R.B. Wilson, and M.L. Kaplan, "Measurement of the Conductor Band Discontinuities of InGaAsP/InP Heterojunctions Using Capacitance-Voltage Analysis," J. Vaccum Sciences Technology, Vol. B4, pp. 37-44, 1986.

24. P. Schuitemaker, P.A. Houston, and P.N. Robson, "Progress on InP/InGaAs(P) Heterojunction Bipolar Transistors," SPIE, Vol. 795, pp. 29-40, 1987.

25. R.N. Nottenburg, H. Temkin, M.B. Panish, R. Bhat, and J.C. Bischoff, "InGaAs/InP Double-Heterostructure Bipolar Transistors With Near-Ideal β Versus I_c Characteristics," IEEE Electron Device Letter, Vol. EDL-7, No. 11, pp. 613-615, November 1986.

26. C.R. Crowell and M. Hafizi, "Current Transport over Parabolic Potentia Barriers in Semiconductor Devices," IEEE Transaction on Electron Devices, Vol.ED-35, No. 7, pp. 1087-1095, July 1988.

27. R. Stratton, "Volt-Current Charactersitcs For Tunneling Through Insulating

Films," J. Phys. Chem. Solids, Vol. 23, pp1177-1190, March 1962.

28. F.A. Padovani and R. Stratton, "Field and Thermionic-Field Emission In Schottky Barriers," Solid State Electronics, Vol. 9, pp. 695-706, 1966.

29. S.C. Lee and H.H. Lin, "Transport Theory of the Double Heterojunction Bipolar Transistor Based On Current Balancing Concept," J. Appl. Phys., Vol. 59, No. 5, pp. 1688-1695, March 1986.

30. H.E. Talley and D.G. Daugherty, "Physical Principles of Semiconductor Devices," The Iowa State University Press, Chapter 7. pp199-202, 1976.

31. Y.G. Chai, C. Yuen, and G.A. Zdasiuk, " Investigation of $In_{0.53}Ga_{0.47}As$ for High-Frequency Microwave Power FET's," IEEE Transaction on Electron Devices, Vol. ED-32, No. 5, pp. 972 - 977, May 1985.

32. M.M. Tashima, L.W. Cook, and G.E. Stiilman, " Minority Carrier Diffusion Lengths In Liquuid Phase Epitaxial InGaAsP and InGaAs," J. Electronic Materials, Vol. 11, No. 4, pp. 831 - 847, 1982.

33. S.R. Forrest and O.K. Kim, "Deep Levels In $In_{0.53}Ga_{0.47}As$/InP Heterostructures," J. Appl. Phys., Vol. 53, No. 8, pp. 5738-5745, August 1982.

34. S.R. Forrest and O.K. Kim, "Analysis of the Dark Current and Photoresponse of $In_{0.51}Ga_{0.47}As$/InP Avalanche Photodiodes," Solid State Electronics, Vol. 26, No. 10, pp. 951-968, 1983.

35. M.J. Ludowise, N. Holongak, P.D. Wright, B.A. Vojak, E.A. Rezek, and H.W. Korb, "Defect- and Phonon-Assited Tunneling in LPE $In_{1-x}Ga_xP_{1-z}As_z$ DH Laser Diodes ($\lambda \approx 1\ \mu m$)," J. Appl. Phys., Vol. 48, No. 10, pp. 4287-4291, October 1977.

36. S. Gourrier, P. Friedel, and J.P. Chane, "Interface Properties of Metal/Oxide/Semiconductor and Metal/Insulator/Semiconductor Structures On $Ga_{1-x}In_xAs$ With x = 0.35 and 0.10," Thin Solid Film, Vol. 103, pp. 155-166, 1983.

37. B. Pejcinovic, T.W. Tang, and D.H. Navon, "High-Frequency Characterization of Heterojunction Bipolar Transistors Using Numerical Simulation," IEEE Transactions on Electron Devices, Vol.ED-36, No. 2, February 1989.

38. M.B. Das, "High-Frequency Performance Limitations of Millimeter-Wave Heterojunction Bipolar Transistors," IEEE Transactions on electron devices, Vol.ED-35, No. 5, May 1988.

40. B. Bayraktaroglu and N. Camilleri, "Microwave Performances of npn and pnp ALGaAs/GaAs Heterojunction Bipolar Transistors," IEEE MTT-S Digest, pp. 529-532, 1988.

The vita has been removed from the scanned document